IEEE Access
Multidisciplinary ⋮ Rapid Review ⋮ Open Access Journal

Received May 4, 2021, accepted May 31, 2021, date of publication June 3, 2021, date of current version June 14, 2021.

Digital Object Identifier 10.1109/ACCESS.2021.3086020

U-Net and Its Variants for Medical Image Segmentation: A Review of Theory and Applications

NAHIAN SIDDIQUE[1], (Graduate Student Member, IEEE), SIDIKE PAHEDING[2], COLIN P. ELKIN[1], (Member, IEEE), AND VIJAY DEVABHAKTUNI[1], (Senior Member, IEEE)

[1]Department of Electrical and Computer Engineering, Purdue University Northwest, Hammond, IN 46323, USA
[2]Department of Applied Computing, Michigan Technological University, Houghton, MI 49931, USA

Corresponding author: Sidike Paheding (spahedin@mtu.edu)

ABSTRACT U-net is an image segmentation technique developed primarily for image segmentation tasks. These traits provide U-net with a high utility within the medical imaging community and have resulted in extensive adoption of U-net as the primary tool for segmentation tasks in medical imaging. The success of U-net is evident in its widespread use in nearly all major image modalities, from CT scans and MRI to X-rays and microscopy. Furthermore, while U-net is largely a segmentation tool, there have been instances of the use of U-net in other applications. Given that U-net's potential is still increasing, this narrative literature review examines the numerous developments and breakthroughs in the U-net architecture and provides observations on recent trends. We also discuss the many innovations that have advanced in deep learning and discuss how these tools facilitate U-net. In addition, we review the different image modalities and application areas that have been enhanced by U-net.

INDEX TERMS Biomedical imaging, deep learning, neural network architecture, segmentation, U-net.

I. INTRODUCTION

Thanks to recent advances in deep learning in computer vision within the past decade, deep learning has been increasingly utilized in the analysis of medical images. While the use of deep learning in computer vision has seen rapid growth in many different fields, it still faces some challenges in the medical imaging field. There have been many breakthrough techniques over the years to overcome these various challenges, and new research is continuously leading to the development of more novel and innovative methods. One such technique that will be discussed in this literature review will be the U-net, a deep learning technique widely adopted within the medical imaging community.

U-net is a neural network architecture designed primarily for image segmentation [1]. The basic structure of a U-net architecture consists of two paths. The first path is the contracting path, also known as the encoder or the analysis path, which is similar to a regular convolution network and provides classification information. The second is an expansion path, also known as the decoder or the synthesis path, consisting of up-convolutions and concatenations with features from the contracting path. This expansion allows the network to learn localized classification information. Additionally, the expansion path also increases the resolution of the output, which can then pass to a final convolutional layer to create a fully segmented image. The resulting network is almost symmetrical, giving it a u-like shape. The main canonical task performed by most convolutional networks is to classify the whole image into a single label. However, classification networks fail to provide pixel-level contextual information, which is of vital importance in medical image analysis. While there have been previous attempts at segmentation tasks, it was not until U-net by Ronneberger *et al.* [1] that a significant improvement in medical image segmentation performance occurred. The U-net network was developed based on the works of Long *et al.* [2] using fully convolutional networks. Their implementation achieved better performance than the previous best on the ISBI 2012 challenge and won the ISBI cell tracking challenge in 2015, beating the state of the art at the time by a considerable margin.

What makes U-net particularly useful is its creation of highly detailed segmentation maps using highly limited

The associate editor coordinating the review of this manuscript and approving it for publication was Junhua Li.

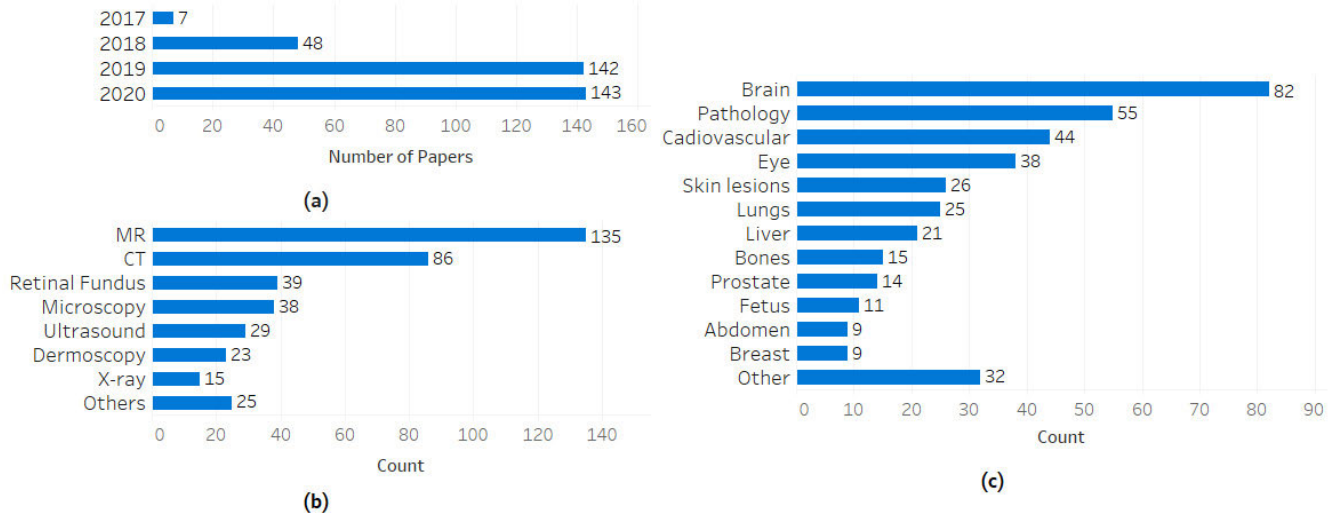

FIGURE 1. Distribution of (a) U-net related papers in our survey by year of publication starting with 2017, (b) image modality in U-net related papers, and (c) application area in U-net related papers. It should be noted that some papers had multiple image modalities and application areas, and each instance was counted separately.

trading samples. The latter trait is of great importance in the medical imaging community, as properly labeled images are often limited. This is achieved by utilizing random elastic deformation on the training data, which enables the network to learn these variations without requiring new labeled data [1]. Another challenge is to separate touching objects of the same class, which is resolved by applying a weighted loss function that penalizes the model if it fails to separate the two objects. Finally, U-net is also much faster to train than most other segmentation models due to its context-based learning.

Since its inception in 2015, U-net has seen an explosion in usage in medical imaging. And naturally, there have been many advancements in U-net architecture by researchers implementing new methods or incorporating other imaging methods into U-net. In this survey, we examine papers that utilize U-net in the application of medical image analysis. To avoid redundancy, we only reviewed papers from 2017 onward. Given that there are numerous sources of scientific publicization, in order to find the most relevant quality of research papers, we limited ourselves to three major publishers: IEEE, Springer, and Elsevier. From there, we searched their databases with related keywords to find the top papers in each database and collected the appropriate publications. Since new papers are being published regularly, we selected a designated endpoint of 12/31/2020. Fig. 1 showcases some statistics from our survey.

II. U-NET ARCHITECTURES

A. BASE U-NET

As mentioned earlier, the U-net network can be divided into two parts: The first is the contracting path that uses a typical CNN architecture. Each block in the contracting path consists of two successive 3×3 convolutions followed by a ReLU activation unit and a max-pooling layer. This arrangement is repeated several times. The novelty of U-net comes in the second part, called the expansive path, in which each stage upsamples the feature map using 2×2 up-convolution. Then, the feature map from the corresponding layer in the contracting path is cropped and concatenated onto the upsampled feature map. This is followed by two successive 3×3 convolutions and ReLU activation. At the final stage, an additional 1×1 convolution is applied to reduce the feature map to the required number of channels and produce the segmented image. The cropping is necessary since pixel features in the edges have the least amount of contextual information and therefore need to be discarded. This results in a network resembling a u-shape and, more importantly, propagates contextual information along the network, which allows it to segment objects in an area using context from a larger overlapping area. Fig. 2 illustrates the overall U-net architecture.

The energy function for the network is given by:

$$E = \sum w(x) \log\left(p_{k(x)}(x)\right) \tag{1}$$

where p_k is the pixel-wise SoftMax function applied over the final feature map, defined as:

$$p_k = \exp(a_k(x)) / \sum_{k'=1}^{K} \exp(a_k(x)') \tag{2}$$

and a_k denotes the activation in channel k.

B. 3D U-NET

3D U-net is an augmentation of the basic U-net framework that enables 3D volumetric segmentation [3]. The core structure still contains a contracting and expansive path. However, all of the 2D operations are replaced with corresponding 3D operations, namely 3D convolutions, 3D max pooling, and 3D up-convolutions, thereby resulting in a three-dimensional

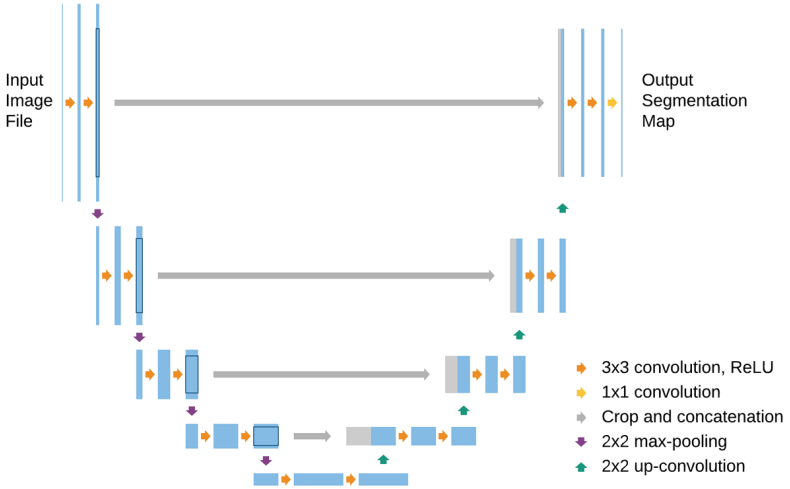

FIGURE 2. Basic U-net architecture. The arrows represent the different operations, the blue boxes represent the feature map at each layer, and the gray boxes represent the cropped feature maps from the contracting path.

segmented image. This network is able to segment images using minimal annotated examples. This is due to 3D images having many repeating structures and shapes, thereby enabling a faster training process even with scarcely labeled data. 3D U-net has seen extensive use in volumetric CT and MR image segmentation applications, including diagnosis of the cardiac structures [4]–[11], bone structures [12]–[15], vertebral column [16], [17], brain tumors [18]–[20], liver tumors [21]–[23], lung nodules [24], nasopharyngeal cancer [25], multi-organ segmentation [26]–[28], head and neck organ at risk assessment [29], and white matter tracts segmentation [30]. 3D U-net has been used to great effect in many biomedical applications. Zeng *et al.* [12] created a network that produced multi-level segmented images that allow abstraction when making a diagnosis.

C. ATTENTION U-NET

An often-desirable trait in an image processing network is the ability to focus on specific objects that are of importance while ignoring unnecessary areas. The attention U-net achieves this by making use of the attention gate [31], [32]. An attention gate is a unit that trims features that are not relevant to the ongoing task. Each layer in the expansive path has an attention gate through which the corresponding features from the contracting path must pass through before the features are concatenated with the upsampled features in the expansive path. Repeated uses of the attention gate after each layer significantly improves segmentation performance without adding excessive computational complexity to the model.

The attention unit is useful in encoder-decoder models such as the U-net since it can provide localized classification information as opposed to global classification. In U-net, this allows different parts of the network to focus on segmenting different objects. Furthermore, with properly labeled training

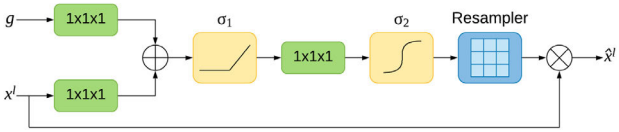

FIGURE 3. Additive attention gate schematic. The input signal xl and the gating signal g both pass through separate 1 × 1 × 1 convolutions. The signals are then added and undergo a series of linear transformation which are ReLU activation ($\sigma 1$), a 1 × 1 × 1 convolution, sigmoid activation ($\sigma 2$), and an optional grid resampler. Finally, the original input is concatenated to the output from the sigmoid unit or the resampler.

data, the network can attune to particular objects in an image. The attention gate applies a function in which the feature map is weighted according to each class, and the network can be tuned to focus on a particular class [33] and hence pay attention to particular objects in an image. While there are different types of attention gates, additive attention is more popular in image processing due to it resulting in higher accuracy [32]. Fig. 3 illustrates a basic additive attention gate. The additive attention gate is described by:

$$q_{att}^{l} = \psi^{T}\left(\sigma_1\left(W_x^{T} x_i^{l} + W_g^{T} g_i + b_g\right)\right) + b_\psi \tag{3}$$

$$\alpha_i^{l} = \sigma_2(q_{att}^{l}(x_i^{l}, g_i; \Theta_{att})) \tag{4}$$

where x^l is the features from the contracting path and g is the gating signal. The term $\sigma_2\left(x_{i,c}\right)$ represents the sigmoid function:

$$\sigma_2\left(x_{i,c}\right) = \frac{1}{1 + \exp(-x_{i,c})} \tag{5}$$

Attention U-net has been successfully applied to problems such as ocular disease diagnosis [34]–[38], melanoma [39], lung cancer [34], cervical cancer [40], abdominal structure segmentation [32], fetus development [32], and brain tissue quantification [41].

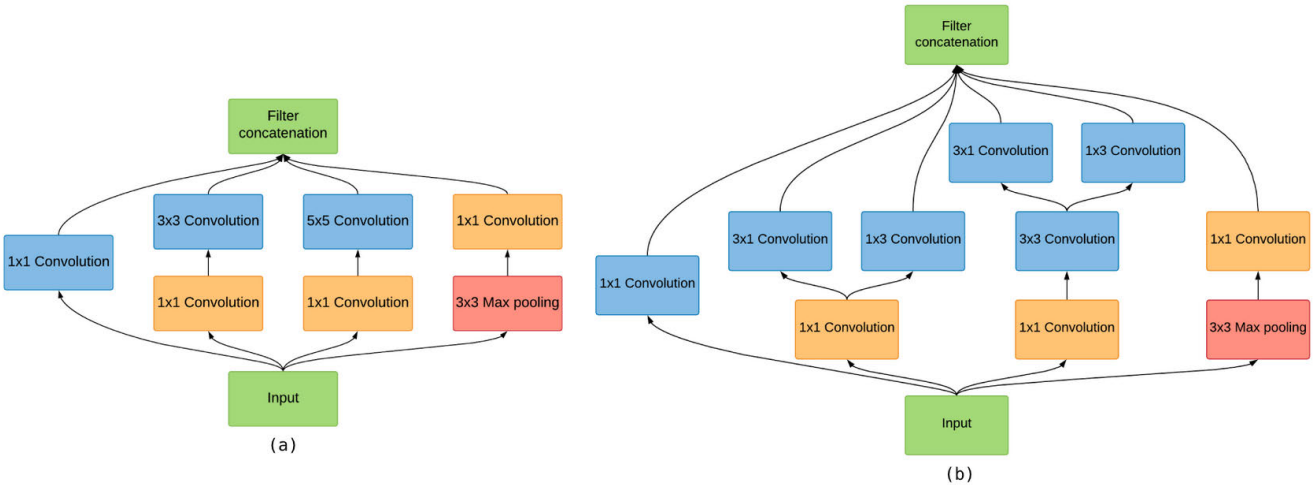

FIGURE 4. (a) The original inception block used in GoogLeNet. (b) Improved inception block with factorized filters. At the end of the inception block, the feature maps from each filter are concatenated together and passed onto the next layer. It should be noted that both networks in figures (a) and (b) are equivalent, though the factorized network requires less computational power.

D. INCEPTION U-NET

Most image processing algorithms tend to use fixed-size filters for convolutions. However, tuning the model to find the correct filter size can often be cumbersome. Moreover, fixed-size filters are appropriate only for images with similar-sized salient parts. In many applications, the analysis looks through images with large variations in shapes and sizes in the salient region. One solution to this problem would be to use deeper networks that can read high-level details across a spectrum of sizes and shapes. However, such deep networks are quite computationally expensive. An alternative solution, called the inception network, uses filters of multiple sizes on the same layer in the network. [42]. The outputs from the different filters are concatenated and transferred onto the next layer. The inception network is able to analyze images with different salient regions quite effectively due to the different filter sizes. To reduce computational complexity, the inception network adds a 1×1 convolution before every 3×3 or larger filter for dimensionality reduction. Additionally, pooling layers may also be added in parallel in each inception module.

The original inception network, called GoogLeNet, attained the state of the art outcomes in the ILSVRC14 competition [42]. This was soon followed by more improvements to the network, including the application of factorization methods and the replacement of 5×5 convolution with two successive 3×3 convolutions. In the latter case, a single 5×5 convolution is 2.78 times more computationally expensive than two equivalent 3×3 convolutions [43]. Further factorization can be applied by splitting $n \times n$ filters into a $1 \times n$ and $n \times 1$ filter, respectively. Factorizing a 3×3 filter by this method makes the network 33% less expensive. Fig. 4 displays two configurations of the inception module.

Inception modules of different configurations have been applied on a multitude of U-net applications, including brain tumor detection [19], [44], [45], brain tissue mapping [46], cardiac segmentation [7], [47], lung nodule detection [48], human embryo segmentation [49], and ultrasound nerve segmentation [50].

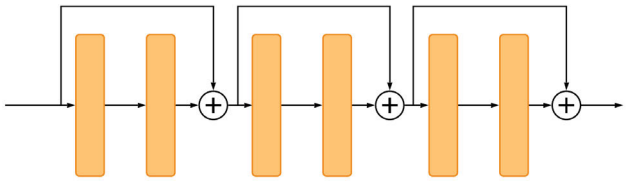

FIGURE 5. Three successive ResNet blocks with skip connections. The skipped signal is joined with the channel output via element-wise addition. The most common ResNet implementations are double-layer skips (as shown in this figure) or triple-layer skips.

E. RESIDUAL U-NET

This variant of U-net is based on the ResNet [51] architecture. The motivation behind ResNet was to overcome the difficulty in training highly deep neural networks. It is known that neural networks are able to converge faster to a solution when more layers are present. However, experimental results have shown that increasing the number of layers results in saturation, and further increases can cause degradation of performance [51]. This degradation arises due to the loss of feature identities in deeper neural networks caused by diminishing gradients in the weight vector. ResNet lessens this problem by utilizing skip connections, which take the feature map from one layer and add it to another layer deeper in the network. This behavior allows the network to better preserve feature maps in deeper neural networks and provide improved performance for such deeper networks. The unit design of ResNet blocks is pictured in Fig 5.

In the residual U-net, at each block in the network, the input to the first convolutional layer is added to the output from the second convolutional layer using a skip connection. This skip

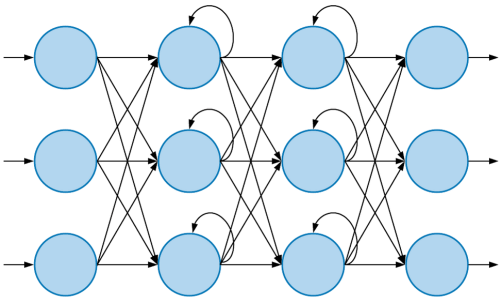

FIGURE 6. Recurrent neural network. In this simple network, the second and third layers are recurrent layers. Each neuron in a recurrent layer receives feedback from its output as well as new information from the previous layer at discrete time periods and correspondingly produces a new output. This component allows the network to process sequential information.

connection is applied before the downsampling or upsampling in the corresponding paths in the U-net. The usage of residual skip connections helps to alleviate the vanishing gradient problem [51], thereby allowing for U-net models with deeper neural networks to be designed. Each residual unit can be denoted by:

$$y_l = h(x_l) + \mathcal{F}(x_l, \mathcal{W}_l) \tag{6}$$

$$x_{l+1} = f(y_l) \tag{7}$$

where x_l and x_{l+1} correspond to the input and output of the residual unit, $\mathcal{F}(\cdot)$ corresponds to the residual function, $f(\cdot)$ is the activation function, and $h(\cdot)$ is the identity mapping function.

We have found papers in which deep residual U-nets have been used to great effect in many biomedical imaging applications such as nuclei segmentation [52], [53], brain tissue quantification [41], brain structure mapping [54], retinal vessel segmentation [55], breast cancer [56], liver cancer [23], [57], prostate cancer [58], endoscopy [59], melanoma [59], osteosarcoma [60], bone structure analysis [61], and cardiac structure analysis [58], [62]. Deep residual U-nets are ideal for complex image analysis.

F. RECURRENT U-NET

Recurrent neural networks are a type of neural network initially designed to analyze sequential data such as text or audio data. The network is designed in such a way that a node's output changes based on the previous output from the same nodes, i.e., a feedback loop as opposed to a traditional feedforward network, as illustrated in Fig. 6. This feedback loop also called a recurrent connection, creates an internal state or memory that provides the node with temporal properties that change the output at discrete time steps. When extended to the entire layer, this allows the network to process contextual information from the preceding data.

The recurrent U-net makes use of recurrent convolutional neural networks (RCNN) [63] by incorporating the recurrent feedback loops into a convolutional layer. The feedback is applied after both convolution and an activation function and feeds the feature map produced by a filter back into the associated layer. The feedback property allows the units to update their feature maps based on context from adjoining units, providing better accuracy and performance. The output y of the recurrent convolutional neural network can be expressed as:

$$y_{ijk}^{l}(t) = \left(w_k^f\right)^T x_l^{f(i,j)}(t) + \left(w_k^r\right)^T x_l^{r(i,j)}(t-1) + b_k \tag{8}$$

where $x_l^f(t)$ is the feedforward input and $x_l^r(t-1)$ is the recurrent input for the l^{th} layer, w_k^f is the feedforward weight, w_k^r is the recurrent weight, and b_k is the bias of the k^{th} feature map. Recurrent U-nets have been used in [64], [65]. Alom *et al.* [52], [66] devised a U-net model containing both recurrent connections and residual connections. The resulting network outperformed solely residual and recurrent U-net models as well as prior state-of-the-art methods using a similar number of parameters.

G. DENSE U-NET

Dense U-nets employ DenseNet [67] blocks in place of regular layers. While the ResNet model allows for deeper neural networks, it does not eliminate the problem of vanishing gradients. The ResNet architecture also eventually degrades in performance with increasing layers. To remedy this, DenseNet is a deep learning architecture built on top of ResNet with two key changes. Firstly, every layer in a block receives the feature or identity map from all of its preceding layers [67]. The second major change is that the identity maps are combined via channel-wise concatenation into tensors [67], as opposed to ResNet, in which the identity maps are summed via element-wise addition. Therefore, the identity mapping of each layer is dependent not only on the previous layer but on all of the layers before it in the block. This configuration is visualized in Fig. 7. This allows DenseNet to preserve all identity maps from prior layers and significantly promote gradient propagation. The implication is that each layer can have fewer channels, as information is more easily preserved between layers, thereby resulting in higher accuracy with fewer computations, which in turn allows deep learning models with a greater number of layers. The output for each layer in a dense block is described as:

$$x_l = H_l([x_0, x_1, x_2, \ldots, x_{l-1}]) \tag{9}$$

where $H_l(\cdot)$ represents the dense mapping function, which typically includes batch normalization, ReLU activation, and a convolutional layer while $[\cdot]$ denotes channel-wise concatenation.

When implementing a U-net, each traditional U-net block is replaced with a dense block of two or more convolutional layers. The adoption of dense blocks allows for deeper U-net models, which can segment objects in an image with greater distinction. This attribute of dense U-nets is highly desired in medical image analysis due to objects in such images being highly close together, often to the point of overlapping. Applications of dense U-net have been found in analysis

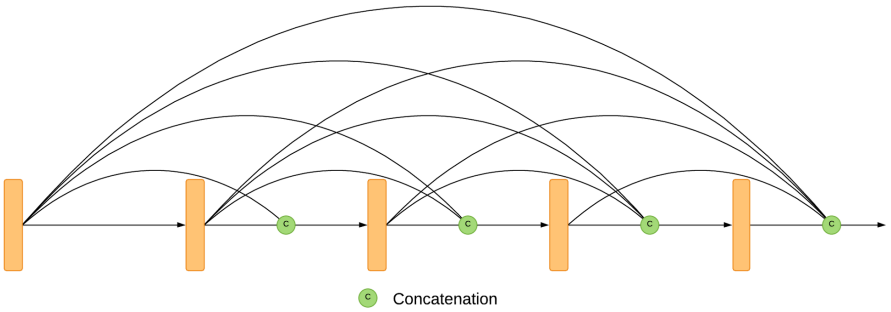

FIGURE 7. A five-layer dense block. The concatenation unit receives the feature map from all previous layers and passes it onto the next layer. This ensures that any given layer has contextual information from any of the previous layers in the block.

of brain tumors [20], [45], retinal blood vessel segmentation [45], cerebral blood vessel segmentation [68], [69], melanoma [70], lung cancer [70], liver cancer [71], and multi-organ segmentation [72].

H. U-NET^{++}

U-net^{++} is another powerful form of the U-net architecture inspired from DenseNet [67]. It uses a dense network of skip connections as an intermediary grid between the contracting and expansive paths [73]. This aids the network by propagating more semantic information between the two paths, thereby enabling it to segment images more accurately.

In traditional U-net, the feature maps of the contracting path are directly concatenated onto the corresponding layers in the expansive path. U-net^{++}, however, has a number of skip connection nodes between each corresponding layer, as represented in Fig. 8. Each skip connection unit receives all of the feature maps from all previous units at the same level, as well as an upsampled feature map from its immediate lower unit. Therefore, each level is equivalent to a dense block. This arrangement minimizes the loss of semantic information between the two paths. The operation of the skip connection unit in which x represents the feature map and i and j correspond to the index down the contracting path and across the skip connections, respectively, is defined as:

$$x^{i,j} = \begin{cases} \mathcal{H}\left(x^{i-1,j}\right), & j = 0 \\ \mathcal{H}\left(\left[\left[x^{i,k}\right]_{k=0}^{j-1}, U\left(x^{i+1,j-1}\right)\right]\right), & j > 0 \end{cases} \tag{10}$$

Here, $\mathcal{H}(\cdot)$ denotes a convolution and the activation operation, $\mathcal{U}(\cdot)$ represents the upsampling operation, and [] signifies a concatenation. The number of intermediary skip connection units depends on the layer number and decreases linearly when traversing the contracting path. Applications in U-net^{++} include segmentation of cell nuclei [73], cancer tissue [73], cardiac structures and vessels [74], [75], and pelvic organs [76].

I. ADVERSARIAL U-NET

An adversarial model is a setup in which two networks compete against each other in order to improve their performance.

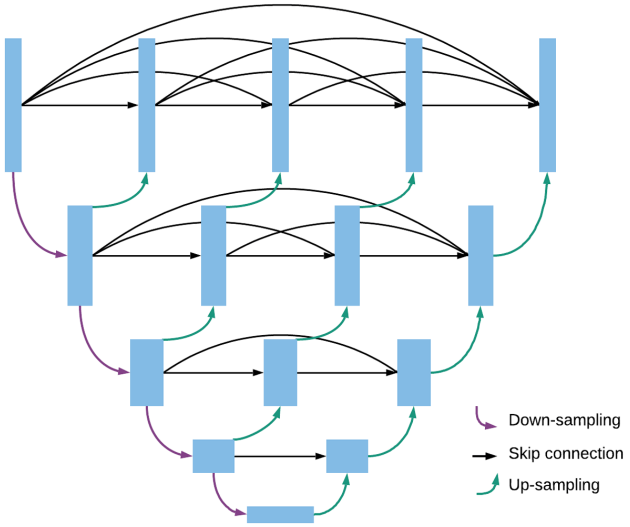

FIGURE 8. U-net++ schematic representation. Each square denotes a convolutional block. Unlike the base U-net, which has a single direct concatenation from the contracting path to the expansive path, U-net++ has a series of intermediary convolutional blocks between the two paths. Each intermediary and expansive block receives the concatenated feature maps from all of the previous blocks at the same level as well as the upsampled feature map from the block immediately below it.

Generative adversarial networks (GAN) are a novel type of adversarial process used to generate new data [77]. The framework consists of two networks: a discriminator and a generator. The discriminator network, D, is a classifier that is trained to identify whether a given input image is from the data set or is produced by the generator G. D undergoes standard CNN supervised training, and for each image input, it outputs the probability of the image being produced by G with the goal of minimizing its error rate of classifying 'fakes' as real data set images. The generator G produces images that are periodically fed to the discriminator. To help the generator produce convincing images, the generator's gradient function is a function of the discriminator's gradient function during the step in which the discriminator is fed a fake image. This allows the generator to adjust its weight in response to the output of the discriminator. Furthermore, to create variations in the images produced by the generator, random noise is passed to it. The goal of the generator is to deceive the

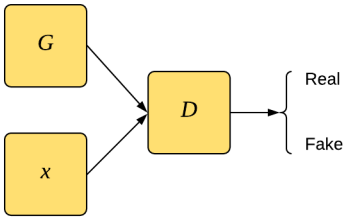

FIGURE 9. GAN block diagram. The goal of network *D* is to classify all inputs from *x* and network *G* as real and fake respectively. The goal of *G* is to have its output evaluated as real.

discriminator, i.e., maximize the error rate of the discriminator. This minimax relationship results in an adversarial network in which the two networks compete with each other, defined as:

$$\min_G \max_D V(D, G) = \mathbb{E}_{x \sim p_{data}(x)} \log D(x) + \mathbb{E}_{z \sim p_z(z)} \log(1 - D(G(z))) \quad (11)$$

where given enough time, the adversarial network should reach an optimal state in which the discriminator always outputs a probability of 1/2 regardless of whether the image is from the data set or the generator [77], meaning that it can no longer distinguish the real images from the synthetic images produced by the generator. The resulting generator can then be used to artificially create images of a particular subject. Fig. 9 presents the basic relational diagram of a GAN.

This framework can be further extended to restrict the GAN into producing a limited band of synthetic images by controlling its labels and input images. This alteration is known as a conditional GAN [78]. Adversarial U-nets are a type of conditional GANs. The generator network is constructed based on the U-net architecture while the discriminator remains the same. The U-net design allows the generator to take an image as an input instead of random noise. The key difference in adversarial U-nets is that the goal of the generator is not to produce new images but rather transformed images. This output of G is evaluated against D, which is trained on manually transformed images. Fig. 10 provides an example of this design. Ideally, after proper training, the generator will be able to achieve the same transformation ability as the manual human transformation. The resulting generator can then be used to apply its transformation function on new images, which would be considerably faster than a physician manually converting the image. Adversarial U-nets have seen a wide spectrum of applications, including quantitative susceptibility mapping of the brain [79], detection of brain tumors [80], [81] and breast cancer [82], segmentation of retinal vessels [38], segmentation of cardiac structures [83], and image registration of brain structures [84].

J. ENSEMBLE U-NET

In addition to the aforementioned architectures, many other network configurations have also been tested that make use of an ensemble of U-nets together. One such method is cascading two or more U-nets. In this arrangement, the first U-net performs a high-level segmentation, with each successive U-net performing segmentation on smaller objects. Feng *et al.* [85] designed a two-stage U-net model in which the first U-net segments the liver from other organs and the second U-net segments tumors within the liver. Liu *et al.* [57] designed a two-stage U-net for liver segmentation with an intermediate processing module between the two U-nets. Xu *et al.* [8] and Li *et al.* [44] have both designed two-stage cascaded U-nets in which the first network is a 2D U-net and the second network is a 3D U-net. Other two-stage U-net models are implemented in [5], [6], [29], [53], [71], [86]–[89]. While two-stage networks are the most common type of cascaded U-nets, we have found two instances of cascaded U-nets with variable numbers of stages [90], [91]. In all of these papers, the cascaded U-net performed better than a single U-net.

Yet another arrangement of the overall architecture can be found in the form of a parallel arrangement of part or the entirety of a U-net network. Abd-Ellah *et al.* [92] arranged two parallel U-nets and aggregated the results for improved segmentation accuracy. Soltanpour *et al.* [93] implemented four parallel U-nets with each segmenting a different CT map and then merging the results. A halfway point can be achieved by parallel encoders, which allow for better extraction of features [94]–[96]. Murugesan *et al.* [97] implemented a network with parallel decoders that provide different levels of segmentation.

2.5D U-net is a special architecture where three 2D U-net networks are run parallelly on different 2D projections of a 3D image to produce a 3D segmentation map. The 2D U-nets perform slice-by-slice segmentation on the 3D volume along three different axes, and the final 3D segmentation is computed by fusing the results [98]–[101]. The advantage of the 2.5D parallel arrangement is reduced computational load for segmentation when juxtaposed with an equivalent 3D network.

K. COMPARISON WITH OTHER ARCHITECTURES

While there have been numerous deep learning models developed for segmentation, in this section, we briefly describe some of the popular alternatives to U-net, namely FCN, Segnet, FPN, and DeepLab. The first deep learning models for semantic segmentation were fully convolutional networks (FCN) [2]. FCNs use regular downsampling paths to extract contextual information and a single upsampling layer to produce a fully segmented image. FCNs also employ optional skip connections; however, due to the design of FCNs, the skipped gradients are often of different dimensions and require additional processing to be upscaled. One of the significant disadvantages of FCNs is their inability to learn global context information [102]. FCNs ultimately fall behind other state-of-the-art segmentation models in terms of performance [102]. Following U-net came Segnet, another encoder-decoder model [103]. However, Segnet does not use skip connections to send low-level contextual information to deeper layers. The main advantage Segnet enjoys over

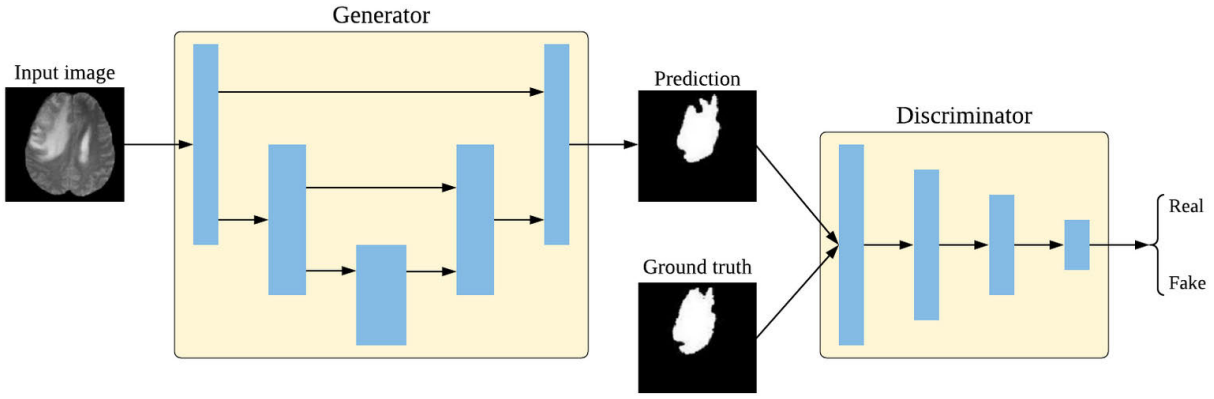

FIGURE 10. Simplified schematic of U-net based GAN. The generator synthesizes predictions for the tumor area from the input images. The predictions are fed into the discriminator, which in turn judges the accuracy of the prediction by evaluating its similarity to the ground truth. If the prediction is similar to the ground truth, then the discriminator will be unable to distinguish between them and classify the prediction as real. Given enough training, the GAN will be able to segment images to the same accuracy and precision as manual annotations [81].

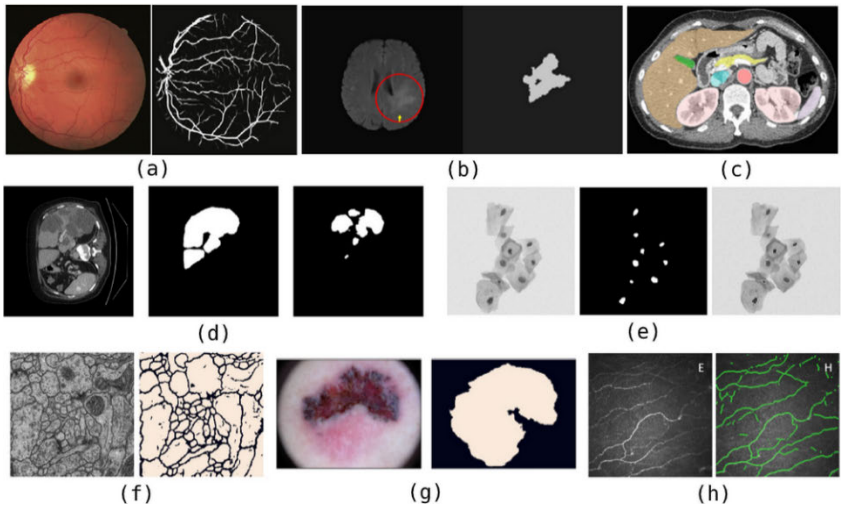

FIGURE 11. Examples of U-net applications. Images have been collected from papers in this survey, including: (a) Retinal vessel segmentation [107]; (b) Brain tumor detection and segmentation [108]; (c) Multi-organ abdominal segmentation (liver; spleen; left and right kidneys; pancreas; gallbladder; aorta; and inferior vena cava) on CT scans [27]; (d) Liver tumor segmentation, left to right: original CT image, liver segmentation image, and lesion segmentation image [109]; (e) Nuclei prediction, from left to right: original cell images, prediction of nuclei, labeling nuclei in the original images [40]; (f) Cell segmentation [59]; (g) Skin lesion segmentation [59]; and (h) Corneal nerve segmentation [110].

other segmentation models is its lower number of training parameters.

Feature pyramid networks (FPN) also have an encoder-decoder structure that was initially designed for object detection [104]. Similar to U-net, here, gradient information is concatenated to the decoder via skip connections from the encoder. However, unlike U-net, the decoder also transmits gradient information from each layer to another series of convolution layers. FPNs are designed to detect objects from each layer in the decoder and are particularly useful in producing multi-class segmentation maps [105]. DeepLab is yet another popular segmentation model that utilizes atrous spatial pyramid pooling [106]. Spatial pyramid pooling enables DeepLab models to take input of different sizes. Atrous or dilated convolution allows the layer to extract contextual information from a larger area without increasing the filter size. Combining these two techniques enables DeepLab models to be highly robust without a significant increase in computational complexity.

III. IMAGE MODALITIES

Segmentation is the primary task for U-net models. The goal of segmentation tasks is to outline and separate different objects in an image, i.e., to classify different objects rather than classifying the whole image. This is of particular importance in the medical imaging community, as the diagnosis of

TABLE 1. Applications of U-net based models for MR image analysis.

Reference	Model/Methods used	Reference	Model/Methods used
Brain tumor		**Cardiovascular structures**	
[111], [112], [115]–[117], [119]–[123], [165]–[171]	Base U-net	[143], [145]–[147], [149], [151], [183], [184]	Base U-net
[18], [114], [125]	3D U-net	[58], [62], [144], [148], [150], [185]	Residual block
[81]	Adversarial net; GAN		
[172]	Attention gate	[4], [9], [10], [28]	3D U-net
[59], [113], [173], [174]	Residual block	[86], [90]	Cascaded U-net
[118]	Dense block	[186]	Attention gate
[175]	U-net++	[5], [8]	Cascaded 3D U-net
[87]	Cascaded U-net	[11], [187]	Base U-net; 3D U-net
[176]	Dense block; Residual block	[83], [188]	Adversarial net; GAN
[177]	3D U-net; Attention gate	[189]	Attention gate; Dense block
[92]	Residual block; Parallel U-net	[190]	3D U-net; Attention gate
[44]	Inception block; Up skip connections	[142]	Dense block
[45]	Dense block; Inception block	[74]	U-net++
[124]	3D U-net; Residual block	[47]	Inception block; Residual block
[19]	3D U-net; Inception block; Residual block	[6]	Cascaded 3D U-net; Residual block
Brain tissue		**Prostate cancer**	
[108], [126]–[129], [178]	Base U-net	[152], [154]–[156], [191]	Base U-net
[28], [179]–[181]	3D U-net	[28]	3D U-net
[182]	2.5D U-net	[187]	Base U-net; 3D U-net
[54]	Residual block	[192]	Attention gate
[101]	Parallel U-net	[188]	Adversarial net; GAN
[41]	Attention gate; Residual block	[64]	Recurrent net
		[58]	Residual block
White matter tracts			
[131], [132]	U-net with modified skip connections	**Liver cancer**	
[130]	Base U-net	[157], [158]	Base U-net
[89]	Cascaded U-net	[21]	3D U-net
		[193]	Attention gate; U-net++
Fetal brain			
[133]–[135]	Base U-net	**Nasopharyngeal cancer**	
[136]	Base U-net; 3D U-net	[25]	3D U-net; Residual block
		[98]	Parallel U-net
Stroke lesion/thrombus		[159]	Modified convolution block
[138]–[141]	Base U-net		
[137]	3D U-net	**Breast cancer**	
[69]	Dense block; Inception block	[160]	Base U-net
		[99]	Parallel U-net
Spinal cord			
[161], [162]	Base U-net	**Blood vessels**	
		[100]	Base U-net
Femur			
[12]–[14]	3D U-net	**Uterus**	
		[164]	Base U-net
Placenta			
[163]	Base U-net	**Vertebral column**	
		[17]	3D U-net

medical conditions requires careful analysis of local regions in an image. For instance, the diagnosis of brain tumors would require separating the tumors from the rest of the brain structures. We have found extensive use of the U-net architecture for a wide assortment of medical imaging analysis. Fig. 11 illustrates some applications of U-net in various areas. In the next section, we discuss the major image modalities on which U-net has been applied.

A. MAGNETIC RESONANCE IMAGING (MRI)

MRI is a very popular radiology imaging technique used to take pictures of soft tissue inside the body. In our review, we have found MRI to be the most popular image modality for segmentation using U-net. MRI is a useful diagnostic tool, particularly for the analysis of the brain. U-net has been used extensively in this regard for the segmentation of brain structures as many different U-net models have been applied on MR images for brain tumor diagnosis [18], [19], [44], [45], [59], [81], [87], [92], [111]–[125]. U-net has also been applied on brain tissue for investigation of neurological conditions [54], [101], [108], [126]–[129], analysis of white matter tissue [89], [130]–[132] fetal brain development [133]–[136], and stroke lesions [69], [137]–[141].

U-net has also been implemented on cardiovascular MR images [4]–[6], [8]–[11], [47], [58], [62], [74], [83], [86], [90], [142]–[151] to segment structures of the heart.

TABLE 2. Applications of U-net based models for CT image analysis.

Reference	Model/Methods used
Liver cancer	
[109], [194], [195], [205]	Base U-net
[22], [28]	3D U-net
[23]	3D U-net; Residual block
[73]	U-net++
[85], [206]	Cascaded U-net
[57]	Cascaded U-net; Residual block
[71]	Cascaded U-net; Dense block
[193]	Attention gate; U-net++
[207]	Dense block; Inception block
[94]	Modified U-net with dual parallel encoders
Cardiovascular structures	
[4]	3D U-net
[221]	Attention gate
[222]	Adversarial net; GAN
[86]	Cascaded U-net
[5]	Cascaded 3D U-net
[124]	3D U-net; Residual block
[7]	3D U-net; Inception block
[75]	U-net++
Bones	
[204]	Base U-net
[14]	3D U-net
[15]	3D U-net; Residual block
[60]	Residual block
[76]	U-net++
Head and neck	
[226]	3D U-net
[29]	Cascaded 3D U-net
Kidney tumor	
[228], [229]	3D U-net
Liver and spleen	
[196]	Dense block
Brain	
[234]	Base U-net
[235]	Attention gate
[46]	Inception block; Residual block
[95]	Modified U-net with dual parallel encoders
Stomach cancer	
[236]	Residual block
Vertebral column	
[237]	Base U-net
[16]	3D U-net

Reference	Model/Methods used
Lung cancer	
[197]–[199], [208]	Base U-net
[209], [210]	3D U-net
[200], [201], [211]–[213]	Residual block
[34]	Attention gate
[24], [214]	3D U-net; Residual block
[48]	Dense block; Inception block
[215]	Dense block; Residual block
[73]	U-net++
Pulmonary tissue	
[216], [217]	Base U-net
[218], [219]	Residual block
Abdominal organs	
[156], [203], [220]	Base U-net
[26], [27]	3D U-net
[32]	Attention gate
[72]	Dense block
Pancreas	
[161], [220], [223], [224]	Base U-net
[28]	3D U-net
Stroke lesions	
[93], [225]	Base U-net
[137]	Base U-net; 3D U-net
[69]	Dense block; Inception block
Gallstones	
[227]	U-net++
[88]	Cascaded U-net
Prostate cancer	
[230]	Base U-net
[231]	Attention gate
Blood vessels	
[232]	Attention gate
[233]	Residual block
Cervical cancer	
[202]	Base U-net
Fetus	
[32]	Attention gate
Melanoma	
[70]	Dense block
Muscle tissue	
[238]	Base U-net

Cancer is a leading cause of death worldwide, and MR is one of the strongest methods for the proper prognosis of different types of cancers. In addition to brain cancer, we have found applications on prostate cancer [58], [64], [152]–[156], liver cancer [21], [157], [158], nasopharyngeal cancer [25], [98], [159], and breast cancer [99], [160]. Other implementations include segmentation of the femur [12]–[14], spinal cord [161], [162], blood vessels [100], vertebral column [17], human placenta [163], and the uterus [164]. Table 1 indexes all of the papers that used MRI as an image mode, as well as the application area and the methods used in the corresponding U-net.

B. COMPUTED TOMOGRAPHY (CT)

CT scans are another major non-invasive medical analysis tool for analyzing internal organs and tissue. As with MRI, cancer diagnosis is a major that involves the application of CT imaging; including liver cancer [22], [23], [57], [71], [73], [85], [94], [109], [194]–[196], lung cancer [24], [34], [45], [48], [70], [73], [197]–[201], bone cancer [60], and cervical cancer [202]. CT scans are also used

TABLE 3. Applications of U-net based models for fundus image analysis.

Reference	Model/Methods used
[107], [239]–[251]	Base U-net
[34]–[36], [232], [252], [253]	Attention gate
[55], [201], [254]–[257]	Residual block
[70]	Dense block
[258]	U-net++
[38]	Adversarial net; GAN; Attention gate
[91]	Cascaded U-net
[259]	Cascaded U-net; Residual block
[260]	Attention gate; Residual block
[45]	Dense block; Inception block
[215], [261]	Dense block; Residual block
[262]	Inception block; Residual block
[263]	Attention gate; Dense block; Residual block
[97]	U-net with parallel decoders
[264]	Recurrent residual block; Up skip connections

for multiorgan abdominal segmentation [26], [27], [32], [72], [156], [203] as well as the segmentation of hard tissue such as bones [14]–[16], [60], [76], [204]. Along with MR imaging, CT is one of the few imaging techniques that can produce 3D images. The versatility of CT imaging makes it a favored modality in medical diagnosis. Table 2 indexes all of the papers that used CT scans as an image mode in our review, as well as the application area and the methods used.

C. RETINAL FUNDUS IMAGING

Color fundus imaging is an ophthalmology technique used for the detection and diagnosis of ocular diseases such as glaucoma, diabetic retinopathy, and age-related macular degeneration (AMD). Proper prognosis depends on the precise segmentation of key structures such as retinal blood vessel segmentation [55], [239]. Accurate screening is of chief importance since such diseases often need to be diagnosed early for treatment. Though ophthalmic imaging has a far narrower scope than MR and CT, the retinal fundus is one of the most analyzed structures in our survey, after the brain and cardiovascular system. Given that it is the primary method of imaging the retina, we expect more research on fundus image analysis to continue as well as research on more complex retinal fundus images. Table 3 collects all of the use cases of U-net models applied in the analysis of the retinal fundus.

D. MICROSCOPY

Microscopy refers to the examination of microscopic objects that cannot be observed with the naked eye. It should be noted that in our survey, we refer to microscopy to mean only optical microscopy. This modality is used extensively in pathology. One of the major challenges in microscopy imaging is identifying overlapping cells as well as identifying the boundary between cells. These are unique challenges to microscopy, as smaller structures such as cells and tissues often do not have well-defined landmarks and similarities, thereby making the image processing much more difficult. However, U-net has overcome such challenges [1] and continues to be a strong implementation for this modality. Applications of U-net based models applied on microscopy imaging are collected and indexed in Table 4.

E. DERMOSCOPY

Dermoscopy is a detailed examination of the skin. It is almost exclusively used to examine skin diseases such as skin lesions. The primary medical condition diagnosed using Dermoscopy images in our survey is melanoma or skin cancer, though we have also found a single paper on psoriasis diagnosis [289]. The performance of Dermoscopy image analysis methods is of keen interest in the medical imaging community since it is often used for early detection of melanoma and is less costly than other noninvasive diagnostic tools. Table 5 summarizes the papers and models focusing on Dermoscopy images.

F. ULTRASOUND

Medical ultrasound is yet another noninvasive imaging technique for the analysis of internal structures. Ultrasound is mostly used for early and real-time diagnosis. Additionally, unlike many other image modalities, ultrasound devices are more maneuverable and can capture images from multiple angles. Ultrasound is also safe since it does not use radiation; hence it is the primary imaging modality for pregnancy-related diagnosis [302]–[304]. Medical ultrasound use cases also include analysis of soft tissue such as nerve bundles [39], [50], [156], [305], [306]. Its real-time image capture abilities make it a vital tool for tracking objects [96]. Applications of U-net in ultrasound imaging are outlined in Table 6.

G. X-RAY

X-ray is a radiograph method used mainly for the imaging of hard tissue. It is the most widely used technique for the analysis of bones. U-net models have been applied to X-rays of bones for diagnosis of rheumatoid arthritis and osteoporosis [61], [324], as well as other bone-related diseases. Chest x-rays are also fairly prevalent and are used for the detection of a myriad of pulmonary diseases such as tuberculosis [260]. Aside from that, we have found applications of U-net in the detection of coronary stenosis [325], breast tumors [82], and surgical catheters [326]. Table 7 encapsulates all of the papers that used X-ray as an image mode for analysis.

H. OTHER MODALITIES

In addition to commonly used image modalities, we have also found U-net applications on more inconspicuous modalities. Endoscopy is an invasive imaging procedure in which the imaging device is inserted into an organ or cavity to take pictures. U-net has been applied to endoscopy images for segmentation of polyps in the gastrointestinal tract [97], [274], [301], [334], colon objects [59], detection of laryngeal leukoplakia [65], and detection of surgical instruments [335]. On electron microscopy images, applications include the detection of neuronal structures [161], [336], cell

TABLE 4. Applications of U-net based models for microscopy image analysis.

Reference	Model/Methods used
Cell nuclei	
[265], [266]	Base U-net
[59], [267], [268]	Residual U-net
[52]	Recurrent net; Residual block
[53]	Cascaded U-net; Residual block
[269]	Cascaded U-net; Dense block
[73]	U-net++
Human embryo	
[277]	Base U-net
[49]	Inception block
Chromosomes	
[278]–[280]	Base U-net
Cancer cell detection	
[285]–[287]	Base U-net
[288]	Residual U-net
Cell contour	
[169], [270]–[273]	Base U-net
[40]	Attention gate
[274]	Cascaded U-net
[275]	Attention gate; Recurrent residual block
[276]	Dense block; Inception block; Residual block
Corneal nerve	
[110]	Base U-net
[36]	Attention gate
Blood vessels	
[281]	Base U-net
Pathogen detection	
[282], [283]	Base U-net
Sclerosis	
[284]	Base U-net

TABLE 5. Applications of U-net based models for Dermoscopy image analysis.

Reference	Model/Methods used
Melanoma	
[248], [290]–[300]	Base U-net
[39]	Attention gate
[59], [213]	Residual block
[70]	Dense block
[260], [301]	Attention gate; Residual block
[263]	Attention gate; Recurrent residual block
[176]	Dense block; Residual block
[274]	Cascaded U-net
[264]	Up skip connections
Psoriasis	
[289]	Base U-net

TABLE 6. Applications of U-net based models for ultrasound image analysis.

Reference	Model/Methods used
Nerve segmentation	
[156], [305]	Base U-net
[50]	Inception block
[306]	Residual block
[307]	Modified parallel U-net
Breast lesion	
[308]	Base U-net
[39], [309]	Attention gate
[310]	Cascaded U-net
Arterial wall	
[311]–[313]	Base U-net
[314]	Cascaded U-net
Cardiovascular structures	
[315]	Base U-net
[170]	Attention gate
[316]	Residual block
Fetal head	
[302], [317]	Base U-net
[318]	Cascaded U-net
Gastrointestinal tumor	
[319]	Base U-net
Knee cartilage	
[96]	U-net with dual parallel encoders
Preterm birth prediction	
[303]	Base U-net
Thyroid	
[320]	Residual block
Transcranial detection	
[304]	Base U-net
Ovary detection	
[321]	Base U-net
Kidney	
[322]	Base U-net
Cervical lymph node	
[323]	Dense block; Residual block; Inception block

contour [161], [201], [232], and viruses [337]. Optical coherence tomography (OCT) is an imaging method for taking cross-sectional images of the retina. OCT is used for the diagnosis of different ocular diseases, such as age-related macular degeneration (AMD), retinal vein occlusion, and diabetic macular edema [338]. U-net has been used on OCT for segmentation of retinal layers [339]–[341], blood vessels [342], fluid regions [343], [344], and Drusen [345]. Other uncommon applications are segmentation of blood vessels in digital subtraction angiography (DSA) [68], [346], [347], white matter tract segmentation in diffusion tensor imaging (DTI) [30], iris segmentation in iris imaging [37], tumor detection in mammograms [56], and capillary segmentation in nailfold capillaroscopy [348]. Table 8 collects the applications of U-net based models on some uncommon image modalities.

IV. OTHER CANONICAL TASKS BY U-NET

Even though U-net is an algorithm developed for segmentation, it has seen a modest amount of augmentation for other types of tasks. Image analysis is often hampered by the presence of noise or loss of detail during imaging. Consequently, we have found three papers

TABLE 7. Applications of U-net based models for X-ray image analysis.

Reference	Model/Methods used
Phalange bones	
[324], [327]	Base U-net
[61]	Residual block
Chest organs	
[328]–[330]	Base U-net
[34], [170]	Attention gate
[260]	Attention gate; Residual block
Pelvic bones	
[331]	Base U-net
Calcaneus bones	
[332]	Base U-net
Blood vessels	
[325], [333]	Base U-net
Breast tumor	
[82]	Adversarial net; GAN
Surgical catheter detection	
[326]	Residual block

TABLE 8. Applications of U-net based models for various image modalities.

Reference	Model/Methods used	Image Modality
[108], [334]	Base U-net	Endoscopy
[59]	Residual block	Endoscopy
[274]	Cascaded U-net	Endoscopy
[301]	Attention gate; Residual block	Endoscopy
[65]	Cascaded U-net; Recurrent residual net	Endoscopy
[97]	Modified U-net with parallel decoders	Endoscopy
[161], [336], [337]	Base U-net	Electron microscopy
[232]	Attention gate	Electron microscopy
[201]	Residual block	Electron microscopy
[338], [341]–[343], [345]	Base U-net	OCT
[339], [340]	Residual block	OCT
[344]	Adversarial net	OCT
[346], [347]	Base U-net	DSA
[68]	Dense block	DSA
[30]	3D U-net	DTI
[37]	Attention gate	Iris imaging
[56]	Residual block	Mammogram
[348]	Residual block	Nailfold capillaroscopy

that implemented U-net to remove artifacts from images by reconstructing the images [79], [349]–[352], as well as a paper that used U-net for de-aliasing [80]. Image registration is also an area in which U-net models have seen experimentation [84], [353]–[356]. Other reconstruction tasks include the correction of infant cortical surface [357] and EPID dosimetry correction of the cerebrospinal region [358]. Other outlier usages include synthesis of medical images [359], image super-resolution [20], and data augmentation for enabling easier annotation of medical images [360]. Applications of U-net based models applied on canonical tasks other than segmentation tasks are summarized in Table 9.

V. NETWORK PERFORMANCE

A. LOSS FUNCTIONS

Aside from network architecture, one of the essential characteristics of a deep learning model is its loss function. In this section, we briefly describe some key loss functions used in image segmentation. One of the most common loss functions used in medical image segmentation is cross-entropy loss.

$$L_{CE} = -\sum_{i=1}^{n} t_i \log(p_i) \tag{12}$$

Here, t_i denotes to the ground truth, p_i denotes the probability for the *ith* class, and n denotes the number of classes [361]. One variant of cross-entropy loss is the weighted cross-entropy loss. This loss function gives certain weights to classes based on class imbalance. Another emerging variant of cross-entropy loss is the focal loss, where well-classified training samples are weighted down.

Besides cross-entropy, the other standard loss function in image segmentation is the Dice loss, obtained from the Sørensen–Dice coefficient [362]. Here GT refers to the ground truth, and SR refers to the segmentation result.

$$Dice = \frac{2\,|GT \cap SR|}{|GT| + |SR|} \tag{13}$$

Intersection over union (IoU) loss, derived from the Jaccard index, measures the ratio of the intersection of the samples to their union [363]. Dice loss and IoU loss are often used to strengthen their respective evaluation metrics.

$$Jaccard/IoU = \frac{|GT \cap SR|}{|GT \cup SR|} \tag{14}$$

Tversky loss is a modification of the Dice loss that gives different weights to false positive and false negative results [364]. This makes it useful in training datasets with unbalanced classes.

$$L = \frac{|GT \cap SR|}{|GT \cap SR| + \alpha\,|SR \backslash GT| + \beta\,|GT \backslash SR|} \tag{15}$$

Lastly, boundary loss is a family of loss functions that aim to minimize the distance between the ground truth and the segmentation results on a regional basis [365]. This loss function is useful for training models on highly unbalanced data.

B. EVALUATION METRICS

As crucial as designing image processing models are, it is equally important to evaluate their performance correctly. In this section, presented are some of the most popular and widely used image segmentation evaluation metrics. Many of these metrics have been derived from the resulting confusion matrix and the associated true positive (TP), true negative (TN), false positive (FP), and false negative (FN) values.

The accuracy metric measures the number of correctly predicted samples against the total number of samples. In image processing, these samples are usually pixels or voxels. Accuracy, however, is not helpful in unbalanced data distributions

TABLE 9. Applications of U-net based models on other canonical tasks.

Reference	Image modality	Canonical task	Model/Methods	Application area
[349]	CT	Denoising	Modified U-net	Cervix
[350]	Ultrasound	Denoising	Base U-net	Brain tissue
[79]	MR	Denoising	3D adversarial net	Brain tumor
[351]	MR	Denoising	Cascaded U-net	Brain tissue
[352]	Photoacoustic tomography	Denoising	Base U-net	Blood vessels
[80]	MR	De-aliasing	Adversarial net	Brain tumor
[353]–[355]	MR	Image registration	Base U-net	Brain tissue
[356]	MR	Image registration	3D U-net	Liver tissue
[84]	MR	Image registration	Adversarial net	Brain tissue
[357]	MR	Image correction	3D U-net	Brain surface
[358]	EPID dosimetry	Image correction	Base U-net	Brain and spinal cord
[359]	CT; MR	Image synthesis	Base U-net	Brain tissue
[360]	MR	Data augmentation	Base U-net	Brain tissue
[20]	MR	Superresolution	3D U-net; Dense block	Brain tumor

that may arise in image processing and is rarely considered by itself [366].

$$Accuracy = \frac{TP + TN}{TP + TN + FP + FN} \tag{16}$$

Precision measures the number of correctly predicted positive samples against all positive predictions. Analogous to precision, specificity measures the number of correctly predicted negative samples among all negative samples. Both precision and specificity are useful to evaluate the number of false positive pixels in an image [366].

$$Precision = \frac{TP}{TP + FP} \tag{17}$$

$$Specificity = \frac{TN}{TN + FP} \tag{18}$$

Recall or sensitivity measures the proportion of positive samples that have been identified correctly as positive. Recall/sensitivity is useful to gauge the number of false negative pixels in an image [366]. It is common practice to pair precision with recall or specificity with sensitivity to get a much broader evaluation of a model or algorithm.

$$Recall/Sensitivity = \frac{TP}{TP + FN} \tag{19}$$

F-score, or F-measure, is the harmonic mean of precision and recall. The F-score is often used to measure the overall performance of a model by combining precision and recall [366].

$$Fscore = \frac{2 \cdot Precision \cdot Recall}{Precision + Recall} \tag{20}$$

The Sørensen–Dice coefficient, commonly known as Dice score, compares the similarity between two samples [362]. Equation 13 describes the Dice score. In binary data evaluation, the Dice score is equivalent to F-score.

The Jaccard index, also known as intersection over union (IoU), is a measure of the overlap between two samples [363]. The Jaccard index is expressed in Equation 14.

The area under curve score (AUC) is another popular metric in image processing, particularly in biomedical image processing. It uses receiver operating characteristics (ROC) to evaluate different thresholds to convert continuous data to discrete data for classification [367]. It is a measure of how easily a model can distinguish between different classes [367].

VI. DISCUSSION

Deep learning techniques such as U-net have seen increasing usage in medical image analysis over the years. Deep learning in image processing has allowed a variety of different tasks such as classification, detection, and localization. Segmentation tasks, however, are of keen interest in the medical imaging community. Surveys conducted by [228], [229] reveal that segmentation is the most sought canonical task in medical image analysis. This is further evident by the abundance of papers published specifically for segmentation tasks, in which U-net and its variants continue to be a prominent method [102]. The examination of U-net in this survey provides some answers to its high utility. In addition to its status as a well-performing segmentation model, a feature of U-net that makes it incredibly valuable is its high modularity and mutability. We have provided in this review numerous papers that have incorporated other deep learning methods into U-net, including some papers that adopt multiple models simultaneously. These alterations alter the low-level architecture of the U-net while retaining the same high-level design. More importantly, this means two things. The first is that this provides U-net a wide spectrum of applications since it can be greatly tuned depending on the application at hand. The second is that U-net still has substantial potential for advancement, since its modular nature allows it to continue improving by incorporating newer novel ideas into itself.

For the specific use cases of this survey, we have found MR to be the most popular image modality, though there remains a healthy variety of other image types. The same holds true for application areas, which successfully implemented U-net for both popular and niche applications. We would also like

to acknowledge the alternate tasks performed in papers in this survey; although they are few, these tasks provide U-net with another avenue for exploration.

A. LIMITATIONS

In this survey, we present the most popular U-net architectures as well as their typical applications. However, it should be highlighted that this survey does not cover all possible U-net variations due to the large body of ongoing research in medical image segmentation. Many other network designs incorporate novel ideas into U-net, such as Bayesian U-net [370] and Capsule U-net [210]. Furthermore, many U-net implementations have hitherto unique modifications, and it is beyond the scope of this survey to cover them all on a case-by-case basis. Nevertheless, we have tried to present the most prevalent and generalized U-net algorithms in this survey.

Additionally, almost all of the U-net architectures surveyed in this study were supervised models. This is ostensible since the majority of medical image segmentation tasks involve supervised learning due to the low acceptable margin of error. Unsupervised U-net models are quite primitive and rare in biomedical imaging; however, there has been steady ongoing research in this area. For completeness, in this section, we present some unsupervised U-net models not limited to the biomedical imaging domain. Xia *et al.* [371] developed a network with two cascaded U-nets, where the reconstruction loss of the whole network and the normalized cut loss of the first U-net is minimized iteratively to saliently segment images. Khan *et al.* [372] designed a dense U-net that segments images via representation oriented clustering. Chen *et al.* [373] developed an attention gated U-net that had promising results on the ISBI 2017 Challenge.

B. CHALLENGES

The success of deep learning is vital for improved medical diagnosis. Although there has been tremendous progress in deep learning techniques such as U-net in the past decade, the nature of medical analysis demands algorithms to perform with minimal error. A major limitation of reducing this error in deep learning techniques is computational power. Powerful deep learning algorithms require more time to train and hence are less feasible. U-net algorithms have applied transfer learning as one solution to alleviate this problem [328]. EfficientNet is a framework for optimizing neural network construction that has the potential to streamline U-net design, thereby making it more powerful using a similar number of parameters [374]. Another critical problem is the scarcity of annotated data for training. Ronneberger *et al.* [1] proposed a solution in their original U-net paper of applying random deformation to create new samples. An alternative solution is the use of adversarial models like GAN to synthesize new image samples. GAN, in particular, has seen tremendous success in synthesizing medical images [375]. Finally, deep learning models have the problem of being 'black boxes'; the input and output to the network are well understood, but the behavior of the internal hidden layers is not. This creates a problem in which researchers often do not understand how to fix errors in the network or which layers or filters are more important to the task. Additionally, black boxes are difficult to interpret properly, and their properties are difficult to replicate [376]. These are some key reasons why deep learning is yet to be used in any large-scale real-world medical trial [377], despite its tremendous promise. However, day by day, these problems are becoming easier to overcome, and we expect to see even greater adoption of deep learning within the medical imaging community in the future. In this regard, we expect U-net to be a major stepping stone in deep learning within the realm of medical image analysis.

C. U-NET FOR COVID-19

The novel coronavirus (COVID-19) pandemic has created a staggering global medical crisis. As of October 2nd, a total of 34,495,176 confirmed cases and 1,025,729 confirmed deaths have been recorded globally [378]. To combat this challenge, the medical imaging community has involved itself in the research of multiple deep learning techniques, including U-net, for the diagnosis of COVID-19. The primary diagnostic images taken for COVID-19 are chest CT scans, which are ideal given that U-net has seen extensive exploration in that modality. The versatility of the U-net network has allowed rapid development and deployment of early screening diagnostic algorithms for field use as early as March 2020 [379]. Further improvements on early screening tests have been made by augmenting attention and residual methods with U-net [380], [381]. Wu *et al.* [382] have implemented a hybrid network with U-net for segmentation and a classifier for classification, while Yan *et al.* [383] developed a network with feature variation that allowed for an easier distinction of COVID-19 infection. U-net research has also been ongoing in X-ray-based screening of COVID-19 [384], [385], and Alom *et al.* [386] established a multi-stage model to detect COVID-19 from X-ray and CT images. A survey on deep learning techniques for COVID-19 diagnosis reveals that U-net is one of the primary models of choice for segmentation-related tasks [387]. This is no surprise, as we have already explored the various utilities of U-net based models. We expect research on U-net-based algorithms for the diagnosis of COVID-19 to continue and to be a major asset to the medical imaging community during this global crisis.

VII. CONCLUSION

In this survey, we aimed to provide a starting point for researchers who wish to explore U-net, which is a powerful deep learning model used extensively for medical image segmentation. To do so, we explored the many variants of U-net and its diverse applications on a multitude of image modalities. We also examined the major deep learning methods and their application areas for all of the papers in this survey. Indeed U-net based architecture is quite ground-breaking and valuable in medical image analysis. The growth of

U-net papers since 2017 lends credence to its status as a premier deep learning technique in medical image diagnosis. Thus, despite the many challenges remaining in deep learning-based image analysis, we expect U-net to be one of the major paths forward.

APPENDIX

A. FRAMEWORKS

There are many open-source deep learning frameworks, among which some of the more popular and widely used frameworks are listed below:

- TensorFlow (Python, C, Java, Go, JavaScript, Swift): https://www.tensorflow.org/
- Keras (Python): https://keras.io/
- PyTorch (Python, C++): https://pytorch.org/
- Caffe (Python, MATLAB): http://caffe.berkeleyvision.org/
- Chainer (Python): https://chainer.org/
- Deeplearning4j (Java, Scala, Python, Clojure, Kotlin): https://deeplearning4j.org/
- Microsoft Cognitive Toolkit (CNTK) (Python, C#, C++): https://docs.microsoft.com/en-us/cognitive-toolkit/
- Theano (Python): http://www.deeplearning.net/software/theano/
- MXNet (Python, Scala, Julia, R, Clojure, Java, C++, Perl): https://mxnet.apache.org/
- ONNX (Python): https://microsoft.github.io/onnxruntime/
- Sonnet (Python): https://github.com/deepmind/sonnet
- PaddlePaddle (Python): https://github.com/PaddlePaddle/Paddle
- DeepGraphLibrary (Python): https://www.dgl.ai/

B. SDK

- NVIDIA CUDA-X AI platforms: https://developer.nvidia.com/deep-learning-software
- Qualcomm mobile platforms: https://developer.qualcomm.com/solutions/artificial-intelligence

C. DATASETS

The following includes some popular benchmarking datasets and databases for medical image segmentation tasks:

- ISBI 2012 cell segmentation challenge: Electron microscopy cell slices. http://brainiac2.mit.edu/isbi_challenge/
- ISBI cell tracking challenge: Database collecting 2D and 3D time-lapse videos of moving cells from past and ongoing ISBI challenges. http://celltrackingchallenge.net/
- LiTS: Liver CT scans for tumor detection. https://competitions.codalab.org/competitions/17094
- LIDC-IDRI: Lung CT scans for cancer detection. https://wiki.cancerimagingarchive.net/display/Public/LIDC-IDRI
- DRIVE: A popular retinal fundus image dataset. https://drive.grand-challenge.org/
- CT Colonography: CT scan dataset for colon cancer detection. https://wiki.cancerimagingarchive.net/display/Public/CT+COLONOGRAPHY
- Kaggle Data Science Bowl 2018: Nuclei segmentation challenge in microscopy images. https://www.kaggle.com/c/data-science-bowl-2018
- ISIC archive: Database of Dermoscopy images from past and ongoing ISIC challenges. https://www.isic-archive.com/
- SICAS Medical Image Repository: Archive for MICCAI Brain Tumor Segmentation Challenge (BRATS), MICCAI Ischemic Stroke Lesion Segmentation Challenge (ISLES), and ISBI Statistical Shape Model Challenge (SHAPE). https://www.smir.ch/Home/Browse
- Medical Segmentation Decathlon: Collection of MR and CT databases for various target areas. http://medicaldecathlon.com/
- OASIS: Brain MRI and PET images. https://www.oasis-brains.org/
- ABIDE: Brain MRI datasets. http://fcon_1000.projects.nitrc.org/indi/abide/
- ICCVB: Prostate MRI and retinal fundus datasets. http://i2cvb.github.io/
- STARE: Retinal fundus dataset. http://cecas.clemson.edu/~ahoover/stare/
- CHASE_DB1: Retinal fundus dataset. https://blogs.kingston.ac.uk/retinal/chasedb1/
- SCR: Chest X-ray dataset. http://www.isi.uu.nl/Research/Databases/SCR/
- DDSM: Mammogram dataset. http://www.eng.usf.edu/cvprg/Mammography/Database.html
- BCDR: Mammogram database. https://bcdr.eu/
- mini-MIAS: Mammogram dataset. http://peipa.essex.ac.uk/info/mias.html
- PanNuke: Histology dataset for nuclei instance segmentation. https://jgamper.github.io/PanNukeDataset/
- University of Cyprus: Multiple sclerosis MRI, teleorthopedics X-ray, and carotid ultrasound datasets. http://www.ehealthlab.cs.ucy.ac.cy/index.php/facilities/32-software/218-datasets
- The cancer imaging archive: A large public repository of cancer image datasets. https://www.cancerimagingarchive.net/
- Cardiac atlas project: Repository of cardiovascular image datasets. http://www.cardiacatlas.org/

D. COVID-19 DATASETS

The following are some publicly available COVID-19 image datasets.

- COVID-CT: https://github.com/UCSD-AI4H/COVID-CT
- COVID-19 CT: http://medicalsegmentation.com/covid19/

- University of Montreal COVID-19 Image Data Collection: https://github.com/ieee8023/covid-chestxray-dataset
- RadiologyAi Consortium: https://www.radiologyaiconsortium.org/view

E. CONFERENCES AND JOURNALS

Listed are some of the top conferences and journals that have been accepting papers on deep learning and computer vision and related fields.

Conferences:

- AAAI Conference on Artificial Intelligence (AAAI)
- British Machine Vision Conference (BMVC)
- Conference on Computer Vision and Pattern Recognition (CVPR)
- European Conference on Computer Vision (ECCV)
- International Conference on Computer Vision (ICCV)
- International Conference on Image Processing (ICIP)
- International Conference on Intelligent Robots and Systems (IROS)
- International Conference on Machine Learning (ICML)
- Medical Image Computing and Computer Assisted Intervention (MICCAI)
- Neural Information Processing Systems (NIPS)

Journals:

- IEEE Transactions on Image Processing
- IEEE Transactions on Medical Imaging
- IEEE Transactions on Pattern Analysis and Machine Intelligence
- International Journal of Computer Vision
- Journal of the American Medical Informatics Association
- Medical Image Analysis

REFERENCES

[1] O. Ronneberger, P. Fischer, and T. Brox, "U-Net: Convolutional networks for biomedical image segmentation," in *Proc. Int. Conf. Med. Image Comput. Comput.-Assist. Intervent.*, 2015, pp. 234–241.

[2] J. Long, E. Shelhamer, and T. Darrell, "Fully convolutional networks for semantic segmentation," in *Proc. IEEE Conf. Comput. Vis. Pattern Recognit. (CVPR)*, Jun. 2015, pp. 3431–3440.

[3] Ö. Çiçek, A. Abdulkadir, S. S. Lienkamp, T. Brox, and O. Ronneberger, "3D U-Net: Learning dense volumetric segmentation from sparse annotation," in *Proc. Int. Conf. Med. Image Comput. Comput.-Assist. Intervent.*, 2016, pp. 424–432.

[4] Q. Tong, M. Ning, W. Si, X. Liao, and J. Qin, "3D deeply-supervised U-Net based whole heart segmentation," in *Proc. Int. Workshop Stat. Atlases Comput. Models Heart*, 2017, pp. 224–232.

[5] C. Wang, T. MacGillivray, G. Macnaught, G. Yang, and D. Newby, "A two-stage U-Net model for 3D multi-class segmentation on full-resolution cardiac data," in *Proc. Int. Workshop Stat. Atlases Comput. Models Heart*, 2018, pp. 191–199.

[6] S. Jia, A. Despinasse, Z. Wang, H. Delingette, X. Pennec, P. Jaïs, H. Cochet, and M. Sermesant, "Automatically segmenting the left atrium from cardiac images using successive 3D U-Nets and a contour loss," in *Proc. Int. Workshop Stat. Atlases Comput. Models Heart*, 2018, pp. 221–229.

[7] S. R. Ravichandran, B. Nataraj, S. Huang, Z. Qin, Z. Lu, A. Katsuki, W. Huang, and Z. Zeng, "3D inception U-Net for aorta segmentation using computed tomography cardiac angiography," in *Proc. IEEE EMBS Int. Conf. Biomed. Health Informat. (BHI)*, May 2019, pp. 1–4.

[8] H. Xu, Z. Xu, W. Gu, and Q. Zhang, "A two-stage fully automatic segmentation scheme using both 2D and 3D U-Net for multi-sequence cardiac MR," in *Proc. Int. Workshop Stat. Atlases Comput. Models Heart*, 2019, pp. 309–316.

[9] T. Wang, J. Xiong, X. Xu, M. Jiang, H. Yuan, M. Huang, J. Zhuang, and Y. Shi, "MSU-Net: Multiscale statistical U-Net for real-time 3D cardiac MRI video segmentation," in *Proc. Int. Conf. Med. Image Comput. Comput.-Assist. Intervent.*, 2019, pp. 614–622.

[10] J. Wu, Y. Zhang, and X. Tang, "Simultaneous tissue classification and lateral ventricle segmentation via a 2D U-Net driven by a 3D fully convolutional neural network," in *Proc. 41st Annu. Int. Conf. IEEE Eng. Med. Biol. Soc. (EMBC)*, Jul. 2019, pp. 5928–5931.

[11] D. Yang, Q. Huang, L. Axel, and D. Metaxas, "Multi-component deformable models coupled with 2D-3D U-Net for automated probabilistic segmentation of cardiac walls and blood," in *Proc. IEEE 15th Int. Symp. Biomed. Imag. (ISBI)*, Apr. 2018, pp. 479–483.

[12] G. Zeng, X. Yang, J. Li, L. Yu, P.-A. Heng, and G. Zheng, "3D U-Net with multi-level deep supervision: Fully automatic segmentation of proximal femur in 3D MR images," in *Proc. Int. Workshop Mach. Learn. Med. Imag.*, 2017, pp. 274–282.

[13] G. Zeng, Q. Wang, T. Lerch, F. Schmaranzer, M. Tannast, K. Siebenrock, and G. Zheng, "Latent3DU-Net: Multi-level latent shape space constrained 3D U-Net for automatic segmentation of the proximal femur from radial MRI of the hip," in *Proc. Int. Workshop Mach. Learn. Med. Imag.*, 2018, pp. 188–196.

[14] G. Zeng and G. Zheng, "3D tiled convolution for effective segmentation of volumetric medical images," in *Proc. Int. Conf. Med. Image Comput. Comput.-Assist. Intervent.*, 2019, pp. 146–154.

[15] J. C. G. Sánchez, M. Magnusson, M. Sandborg, Å. C. Tedgren, and A. Malusek, "Segmentation of bones in medical dual-energy computed tomography volumes using the 3D U-Net," *Phys. Med.*, vol. 69, pp. 241–247, Jan. 2020.

[16] H.-J. Bae, H. Hyun, Y. Byeon, K. Shin, Y. Cho, Y. J. Song, S. Yi, S.-U. Kuh, J. S. Yeom, and N. Kim, "Fully automated 3D segmentation and separation of multiple cervical vertebrae in CT images using a 2D convolutional neural network," *Comput. Methods Programs Biomed.*, vol. 184, Feb. 2020, Art. no. 105119.

[17] C. Wang, Y. Guo, W. Chen, and Z. Yu, "Fully automatic intervertebral disc segmentation using multimodal 3D U-Net," in *Proc. IEEE 43rd Annu. Comput. Softw. Appl. Conf. (COMPSAC)*, Jul. 2019, pp. 730–739.

[18] R. Mehta and T. Arbel, "3D U-Net for brain tumour segmentation," in *Proc. Int. MICCAI Brainlesion Workshop*, 2018, pp. 254–266.

[19] W. Chen, B. Liu, S. Peng, J. Sun, and X. Qiao, "S3D-UNet: Separable 3D U-Net for brain tumor segmentation," in *Proc. Int. MICCAI Brainlesion Workshop*, 2018, pp. 358–368.

[20] M. Kolarik, R. Burget, V. Uher, and L. Povoda, "Superresolution of MRI brain images using unbalanced 3D dense-U-Net network," in *Proc. 42nd Int. Conf. Telecommun. Signal Process. (TSP)*, Jul. 2019, pp. 643–646.

[21] J. Owler, B. Irving, G. Ridgeway, M. Wojciechowska, J. McGonigle, and M. Brady, "Comparison of multi-atlas segmentation and U-Net approaches for automated 3D liver delineation in MRI," in *Proc. Annu. Conf. Med. Image Understand. Anal.*, 2019, pp. 478–488.

[22] Q. Huang, J. Sun, H. Ding, X. Wang, and G. Wang, "Robust liver vessel extraction using 3D U-Net with variant dice loss function," *Comput. Biol. Med.*, vol. 101, pp. 153–162, Oct. 2018.

[23] W. Yu, B. Fang, Y. Liu, M. Gao, S. Zheng, and Y. Wang, "Liver vessels segmentation based on 3d residual U-Net," in *Proc. IEEE Int. Conf. Image Process. (ICIP)*, Sep. 2019, pp. 250–254.

[24] C. Zhao, J. Han, Y. Jia, and F. Gou, "Lung nodule detection via 3D U-Net and contextual convolutional neural network," in *Proc. Int. Conf. Netw. Netw. Appl. (NaNA)*, Oct. 2018, pp. 356–361.

[25] Y. He, X. Yu, C. Liu, J. Zhang, K. Hu, and H. C. Zhu, "A 3D dual path U-Net of cancer segmentation based on MRI," in *Proc. IEEE 3rd Int. Conf. Image, Vis. Comput. (ICIVC)*, Jun. 2018, pp. 268–272.

[26] M. P. Heinrich, O. Oktay, and N. Bouteldja, "OBELISK-Net: Fewer layers to solve 3D multi-organ segmentation with sparse deformable convolutions," *Med. Image Anal.*, vol. 54, pp. 1–9, May 2019.

[27] H. Kakeya, T. Okada, and Y. Oshiro, "3D U-JAPA-Net: Mixture of convolutional networks for abdominal multi-organ CT segmentation," in *Proc. Int. Conf. Med. Image Comput. Comput.-Assist. Intervent.*, 2018, pp. 426–433.

[28] C. Huang, H. Han, Q. Yao, S. Zhu, and S. K. Zhou, "3D U^2-Net: A 3D universal U-Net for multi-domain medical image segmentation," in *Proc. Int. Conf. Med. Image Comput. Comput.-Assist. Intervent.*, 2019, pp. 291–299.

[29] Y. Wang, L. Zhao, M. Wang, and Z. Song, "Organ at risk segmentation in head and neck CT images using a two-stage segmentation framework based on 3D U-Net," *IEEE Access*, vol. 7, pp. 144591–144602, 2019.

[30] B. Li, M. de Groot, M. W. Vernooij, M. A. Ikram, W. J. Niessen, and E. E. Bron, "Reproducible white matter tract segmentation using 3D U-Net on a large-scale DTI dataset," in *Proc. Int. Workshop Mach. Learn. Med. Imag.*, 2018, pp. 205–213.

[31] O. Oktay, J. Schlemper, L. Le Folgoc, M. Lee, M. Heinrich, K. Misawa, K. Mori, S. McDonagh, N. Y Hammerla, B. Kainz, B. Glocker, and D. Rueckert, "Attention U-Net: Learning where to look for the pancreas," 2018, *arXiv:1804.03999*. [Online]. Available: http://arxiv.org/abs/1804.03999

[32] J. Schlemper, O. Oktay, M. Schaap, M. Heinrich, B. Kainz, B. Glocker, and D. Rueckert, "Attention gated networks: Learning to leverage salient regions in medical images," *Med. Image Anal.*, vol. 53, pp. 197–207, Apr. 2019.

[33] A. Vaswani, N. Shazeer, N. Parmar, J. Uszkoreit, L. Jones, A. N. Gomez, L. Kaiser, and I. Polosukhin, "Attention is all you need," in *Proc. Adv. Neural Inf. Process. Syst.*, 2017, pp. 5998–6008.

[34] Z. Zhang, H. Fu, H. Dai, J. Shen, Y. Pang, and L. Shao, "ET-Net: A generic edge-attention guidance network for medical image segmentation," in *Proc. Int. Conf. Med. Image Comput. Comput.-Assist. Intervent.*, 2019, pp. 442–450.

[35] Z. Si, D. Fu, and J. Li, "U-Net with attention mechanism for retinal vessel segmentation," in *Image and Graphics*. Cham, Switzerland: Springer, 2019, pp. 668–677.

[36] L. Mou, Y. Zhao, L. Chen, J. Cheng, Z. Gu, H. Hao, H. Qi, Y. Zheng, A. Frangi, and J. Liu, "CS-Net: Channel and spatial attention network for curvilinear structure segmentation," in *Medical Image Computing and Computer Assisted Intervention*. Cham, Switzerland: Springer, 2019, pp. 721–730.

[37] S. Lian, Z. Luo, Z. Zhong, X. Lin, S. Su, and S. Li, "Attention guided U-Net for accurate iris segmentation," *J. Vis. Commun. Image Represent.*, vol. 56, pp. 296–304, Oct. 2018.

[38] C. Wu, Y. Zou, and Z. Yang, "U-GAN: Generative adversarial networks with U-Net for retinal vessel segmentation," in *Proc. 14th Int. Conf. Comput. Sci. Educ. (ICCSE)*, Aug. 2019, pp. 642–646, doi: 10.1109/ICCSE.2019.8845397.

[39] N. Abraham and N. M. Khan, "A novel focal tversky loss function with improved attention U-Net for lesion segmentation," in *Proc. IEEE 16th Int. Symp. Biomed. Imag. (ISBI)*, Apr. 2019, pp. 683–687.

[40] H. Zhang, H. Zhu, and X. Ling, "Polar coordinate sampling-based segmentation of overlapping cervical cells using attention U-Net and random walk," *Neurocomputing*, vol. 383, pp. 212–223, Mar. 2020.

[41] Z. Fang, Y. Chen, D. Nie, W. Lin, and D. Shen, "RCA-U-Net: Residual channel attention U-Net for fast tissue quantification in magnetic resonance fingerprinting," in *Proc. Int. Conf. Med. Image Comput. Comput.-Assist. Intervent.*, 2019, pp. 101–109.

[42] C. Szegedy, W. Liu, Y. Jia, P. Sermanet, S. Reed, D. Anguelov, D. Erhan, V. Vanhoucke, and A. Rabinovich, "Going deeper with convolutions," in *Proc. IEEE Conf. Comput. Vis. Pattern Recognit. (CVPR)*, Jun. 2015, pp. 1–9.

[43] C. Szegedy, V. Vanhoucke, S. Ioffe, J. Shlens, and Z. Wojna, "Rethinking the inception architecture for computer vision," in *Proc. IEEE Conf. Comput. Vis. Pattern Recognit. (CVPR)*, Jun. 2016, pp. 2818–2826.

[44] H. Li, A. Li, and M. Wang, "A novel end-to-end brain tumor segmentation method using improved fully convolutional networks," *Comput. Biol. Med.*, vol. 108, pp. 150–160, May 2019.

[45] Z. Zhang, C. Wu, S. Coleman, and D. Kerr, "DENSE-INception U-Net for medical image segmentation," *Comput. Methods Programs Biomed.*, vol. 192, Aug. 2020, Art. no. 105395.

[46] L. Chen, P. Bentley, K. Mori, K. Misawa, M. Fujiwara, and D. Rueckert, "DRINet for medical image segmentation," *IEEE Trans. Med. Imag.*, vol. 37, no. 11, pp. 2453–2462, Nov. 2018.

[47] A. H. Curiale, F. D. Colavecchia, and G. Mato, "Automatic quantification of the LV function and mass: A deep learning approach for cardiovascular MRI," *Comput. Methods Programs Biomed.*, vol. 169, pp. 37–50, Feb. 2019.

[48] H. Cheng, Y. Zhu, and H. Pan, "Modified U-Net block network for lung nodule detection," in *Proc. IEEE 8th Joint Int. Inf. Technol. Artif. Intell. Conf. (ITAIC)*, May 2019, pp. 599–605.

[49] R. M. Rad, P. Saeedi, J. Au, and J. Havelock, "Trophectoderm segmentation in human embryo images via inceptioned U-Net," *Med. Image Anal.*, vol. 62, May 2020, Art. no. 101612.

[50] H. Zhao and N. Sun, "Improved U-Net model for nerve segmentation," in *Image and Graphics*. Cham, Switzerland: Springer, 2017, pp. 496–504.

[51] K. He, X. Zhang, S. Ren, and J. Sun, "Deep residual learning for image recognition," in *Proc. IEEE Conf. Comput. Vis. Pattern Recognit. (CVPR)*, Jun. 2016, pp. 770–778.

[52] M. Z. Alom, C. Yakopcic, T. M. Taha, and V. K. Asari, "Nuclei segmentation with recurrent residual convolutional neural networks based U-Net (R2U-Net)," in *Proc. IEEE Nat. Aerosp. Electron. Conf. (NAECON)*, Jul. 2018, pp. 228–233.

[53] S. Das, A. Deka, Y. Iwahori, M. K. Bhuyan, T. Iwamoto, and J. Ueda, "Contour-aware residual W-Net for nuclei segmentation," *Procedia Comput. Sci.*, vol. 159, pp. 1479–1488, Jan. 2019.

[54] H. Li, A. Zhygallo, and B. Menze, "Automatic brain structures segmentation using deep residual dilated U-Net," in *Proc. Int. MICCAI Brainlesion Workshop*, 2018, pp. 385–393.

[55] T. Mostafiz, I. Jarin, S. A. Fattah, and C. Shahnaz, "Retinal blood vessel segmentation using residual block incorporated U-Net architecture and fuzzy inference system," in *Proc. IEEE Int. WIE Conf. Electr. Comput. Eng. (WIECON-ECE)*, Dec. 2018, pp. 106–109, doi: 10.1109/WIECON-ECE.2018.8783182.

[56] H. Li, D. Chen, W. H. Nailon, M. E. Davies, and D. Laurenson, "Improved breast mass segmentation in mammograms with conditional residual U-Net," in *Image Analysis for Moving Organ, Breast, and Thoracic Images*. Cham, Switzerland: Springer, 2018, pp. 81–89.

[57] Y. Liu, N. Qi, Q. Zhu, and W. Li, "CR-U-Net: Cascaded U-Net with residual mapping for liver segmentation in CT Images," in *Proc. IEEE Vis. Commun. Image Process. (VCIP)*, Dec. 2019, pp. 1–4.

[58] M. Baldeon-Calisto and S. K. Lai-Yuen, "AdaResU-Net: Multiobjective adaptive convolutional neural network for medical image segmentation," *Neurocomputing*, vol. 392, pp. 325–340, Jun. 2020.

[59] N. Ibtehaz and M. S. Rahman, "MultiResUNet: Rethinking the U-Net architecture for multimodal biomedical image segmentation," *Neural Netw.*, vol. 121, pp. 74–87, Jan. 2020.

[60] R. Zhang, L. Huang, W. Xia, B. Zhang, B. Qiu, and X. Gao, "Multiple supervised residual network for osteosarcoma segmentation in CT images," *Comput. Med. Imag. Graph.*, vol. 63, pp. 1–8, Jan. 2018.

[61] K. Kawagoe, K. Hatano, S. Murakami, H. Lu, H. Kim, and T. Aoki, "Automatic segmentation method of phalange regions based on residual U-Net and MSGVF snakes," in *Proc. 19th Int. Conf. Control, Automat. Syst. (ICCAS)*, Oct. 2019, pp. 1046–1049, doi: 10.23919/ICCAS47443.2019.8971740.

[62] E. Kerfoot, J. Clough, I. Oksuz, J. Lee, A. P. King, and J. A. Schnabel, "Left-ventricle quantification using residual U-Net," in *Proc. Int. Workshop Stat. Atlases Comput. Models Heart*, 2018, pp. 371–380.

[63] M. Liang and X. Hu, "Recurrent convolutional neural network for object recognition," in *Proc. IEEE Conf. Comput. Vis. Pattern Recognit. (CVPR)*, Jun. 2015, pp. 3367–3375.

[64] P. Q. Lee, A. Guida, S. Patterson, T. Trappenberg, C. Bowen, S. D. Beyea, J. Merrimen, C. Wang, and S. E. Clarke, "Model-free prostate cancer segmentation from dynamic contrast-enhanced MRI with recurrent convolutional networks: A feasibility study," *Comput. Med. Imag. Graph.*, vol. 75, pp. 14–23, Jul. 2019.

[65] B. Ji, J. Ren, X. Zheng, C. Tan, R. Ji, Y. Zhao, and K. Liu, "A multiscale recurrent fully convolution neural network for laryngeal leukoplakia segmentation," *Biomed. Signal Process. Control*, vol. 59, May 2020, Art. no. 101913.

[66] M. Z. Alom, M. Hasan, C. Yakopcic, T. M. Taha, and V. K. Asari, "Recurrent residual convolutional neural network based on U-Net (R2U-Net) for medical image segmentation," 2018, *arXiv:1802.06955*. [Online]. Available: http://arxiv.org/abs/1802.06955

[67] G. Huang, Z. Liu, L. Van Der Maaten, and K. Q. Weinberger, "Densely connected convolutional networks," in *Proc. IEEE Conf. Comput. Vis. Pattern Recognit. (CVPR)*, Jul. 2017, pp. 4700–4708.

[68] C. Meng, K. Sun, S. Guan, Q. Wang, R. Zong, and L. Liu, "Multiscale dense convolutional neural network for DSA cerebrovascular segmentation," *Neurocomputing*, vol. 373, pp. 123–134, Jan. 2020.

[69] J. Dolz, I. B. Ayed, and C. Desrosiers, "Dense multi-path U-Net for ischemic stroke lesion segmentation in multiple image modalities," in *Proc. Int. MICCAI Brainlesion Workshop*, 2018, pp. 271–282.

[70] R. Azad, M. Asadi-Aghbolaghi, M. Fathy, and S. Escalera, "Bi-directional ConvLSTM U-Net with densley connected convolutions," in *Proc. IEEE/CVF Int. Conf. Comput. Vis. Workshop (ICCVW)*, Oct. 2019, pp. 1–10.

[71] X. Li, H. Chen, X. Qi, Q. Dou, C.-W. Fu, and P.-A. Heng, "H-DenseUNet: Hybrid densely connected UNet for liver and tumor segmentation from CT volumes," *IEEE Trans. Med. Imag.*, vol. 37, no. 12, pp. 2663–2674, Dec. 2018.

[72] Z.-H. Wang, Z. Liu, Y.-Q. Song, and Y. Zhu, "Densely connected deep U-Net for abdominal multi-organ segmentation," in *Proc. IEEE Int. Conf. Image Process. (ICIP)*, Sep. 2019, pp. 1415–1419.

[73] Z. Zhou, M. M. R. Siddiquee, N. Tajbakhsh, and J. Liang, "UNet++: A nested U-Net architecture for medical image segmentation," in *Deep Learning in Medical Image Analysis and Multimodal Learning for Clinical Decision Support*. Cham, Switzerland: Springer, 2018, pp. 3–11.

[74] J. Ren, H. Sun, Y. Huang, and H. Gao, "Knowledge-based multi-sequence MR segmentation via deep learning with a hybrid U-Net++ model," in *Proc. Int. Workshop Stat. Atlases Comput. Models Heart*, 2019, pp. 280–289.

[75] H. Cui, X. Liu, and N. Huang, "Pulmonary vessel segmentation based on orthogonal fused U-Net++ of chest CT images," in *Proc. Int. Conf. Med. Image Comput. Comput.-Assist. Intervent.*, 2019, pp. 293–300.

[76] S. Wu, Z. Wang, C. Liu, C. Zhu, S. Wu, and K. Xiao, "Automatical segmentation of pelvic organs after hysterectomy by using dilated convolution U-Net++," in *Proc. IEEE 19th Int. Conf. Softw. Qual., Rel. Secur. Companion (QRS-C)*, Jul. 2019, pp. 362–367.

[77] I. Goodfellow, J. Pouget-Abadie, M. Mirza, B. Xu, D. Warde-Farley, S. Ozair, A. Courville, and Y. Bengio, "Generative adversarial nets," in *Proc. 27th Int. Conf. Neural Inf. Process. Syst.*, 2014, pp. 2672–2680.

[78] M. Mirza and S. Osindero, "Conditional generative adversarial nets," 2014, *arXiv:1411.1784*. [Online]. Available: http://arxiv.org/abs/1411.1784

[79] Y. Chen, A. Jakary, S. Avadiappan, C. P. Hess, and J. M. Lupo, "QSM-GAN: Improved quantitative susceptibility mapping using 3D generative adversarial networks with increased receptive field," *NeuroImage*, vol. 207, Feb. 2020, Art. no. 116389.

[80] G. Yang, S. Yu, H. Dong, G. Slabaugh, P. L. Dragotti, X. Ye, F. Liu, S. Arridge, J. Keegan, Y. Guo, and D. Firmin, "DAGAN: Deep de-aliasing generative adversarial networks for fast compressed sensing MRI reconstruction," *IEEE Trans. Med. Imag.*, vol. 37, no. 6, pp. 1310–1321, Jun. 2018.

[81] Y. Xue, T. Xu, H. Zhang, L. R. Long, and X. Huang, "SegAN: Adversarial network with multi-scale l1 loss for medical image segmentation," *Neuroinformatics*, vol. 16, nos. 3–4, pp. 383–392, Oct. 2018.

[82] T. Shen, C. Gou, F.-Y. Wang, Z. He, and W. Chen, "Learning from adversarial medical images for X-ray breast mass segmentation," *Comput. Methods Programs Biomed.*, vol. 180, Oct. 2019, Art. no. 105012, doi: 10.1016/j.cmpb.2019.105012.

[83] R. R. Upendra, S. Dangi, and C. A. Linte, "An adversarial network architecture using 2D U-Net models for segmentation of left ventricle from cine cardiac MRI," in *Proc. Int. Conf. Funct. Imag. Modeling Heart*, 2019, pp. 415–424.

[84] G. Li, L. Zhang, S. Hu, D. Fu, and M. Liu, "Adversarial network with dual U-Net model and multiresolution loss computation for medical images registration," in *Proc. 12th Int. Congr. Image Signal Process., Biomed. Eng. Informat. (CISP-BMEI)*, Oct. 2019, pp. 1–5.

[85] X. Feng, C. Wang, S. Cheng, and L. Guo, "Automatic liver and tumor segmentation of CT based on cascaded U-Net," in *Proc. Chin. Intell. Syst. Conf.*, 2019, pp. 155–164.

[86] T. Liu, Y. Tian, S. Zhao, X. Huang, and Q. Wang, "Automatic whole heart segmentation using a two-stage U-Net framework and an adaptive threshold window," *IEEE Access*, vol. 7, pp. 83628–83636, 2019.

[87] H. Liu, X. Shen, F. Shang, F. Ge, and F. Wang, "CU-Net: Cascaded U-Net with loss weighted sampling for brain tumor segmentation," in *Multimodal Brain Image Analysis and Mathematical Foundations of Computational Anatomy*. Cham, Switzerland: Springer, 2019, pp. 102–111.

[88] X. Fu, N. Cai, K. Huang, H. Wang, P. Wang, C. Liu, and H. Wang, "M-Net: A novel U-Net with multi-stream feature fusion and multi-scale dilated convolutions for bile ducts and hepatolith segmentation," *IEEE Access*, vol. 7, pp. 148645–148657, 2019.

[89] J. Hong, B.-Y. Park, M. J. Lee, C.-S. Chung, J. Cha, and H. Park, "Two-step deep neural network for segmentation of deep white matter hyperintensities in migraineurs," *Comput. Methods Programs Biomed.*, vol. 183, Jan. 2020, Art. no. 105065.

[90] D. M. Vigneault, W. Xie, C. Y. Ho, D. A. Bluemke, and J. A. Noble, "Ω-Net (omega-net): Fully automatic, multi-view cardiac MR detection, orientation, and segmentation with deep neural networks," *Med. Image Anal.*, vol. 48, pp. 95–106, Aug. 2018.

[91] J. Hu, H. Wang, S. Gao, M. Bao, T. Liu, Y. Wang, and J. Zhang, "S-UNet: A bridge-style U-Net framework with a saliency mechanism for retinal vessel segmentation," *IEEE Access*, vol. 7, pp. 174167–174177, 2019, doi: 10.1109/ACCESS.2019.2940476.

[92] M. K. Abd-Ellah, A. A. Khalaf, A. I. Awad, and H. F. Hamed, "TPUAR-Net: Two parallel U-Net with asymmetric residual-based deep convolutional neural network for brain tumor segmentation," in *Proc. Int. Conf. Image Anal. Recognit.*, 2019, pp. 106–116.

[93] M. Soltanpour, R. Greiner, P. Boulanger, and B. Buck, "Ischemic stroke lesion prediction in CT perfusion scans using multiple parallel U-Nets following by a pixel-level classifier," in *Proc. IEEE 19th Int. Conf. Bioinf. Bioeng. (BIBE)*, Oct. 2019, pp. 957–963.

[94] L. Zhang and L. Xu, "An automatic liver segmentation algorithm for CT images U-Net with separated paths of feature extraction," in *Proc. IEEE 3rd Int. Conf. Image, Vis. Comput. (ICIVC)*, Jun. 2018, pp. 294–298.

[95] D. Kwon, J. Ahn, J. Kim, I. Choi, S. Jeong, Y.-S. Lee, J. Park, and M. Lee, "Siamese U-Net with healthy template for accurate segmentation of intracranial hemorrhage," in *Proc. Int. Conf. Med. Image Comput. Comput.-Assist. Intervent.*, 2019, pp. 848–855.

[96] M. Dunnhofer, M. Antico, F. Sasazawa, Y. Takeda, S. Camps, N. Martinel, C. Micheloni, G. Carneiro, and D. Fontanarosa, "Siam-U-Net: Encoder-decoder siamese network for knee cartilage tracking in ultrasound images," *Med. Image Anal.*, vol. 60, Feb. 2020, Art. no. 101631, doi: 10.1016/j.media.2019.101631.

[97] B. Murugesan, K. Sarveswaran, S. M. Shankaranarayana, K. Ram, J. Joseph, and M. Sivaprakasam, "Psi-Net: Shape and boundary aware joint multi-task deep network for medical image segmentation," in *Proc. 41st Annu. Int. Conf. IEEE Eng. Med. Biol. Soc. (EMBC)*, Jul. 2019, pp. 7223–7226.

[98] K. Hu, C. Liu, X. Yu, J. Zhang, Y. He, and H. Zhu, "A 2.5D cancer segmentation for MRI images based on U-Net," in *Proc. 5th Int. Conf. Inf. Sci. Control Eng. (ICISCE)*, Jul. 2018, pp. 6–10.

[99] G. Piantadosi, M. Sansone, R. Fusco, and C. Sansone, "Multi-planar 3D breast segmentation in MRI via deep convolutional neural networks," *Artif. Intell. Med.*, vol. 103, Mar. 2020, Art. no. 101781.

[100] C. Angermann and M. Haltmeier, "Random 2.5 D U-Net for fully 3D segmentation," in *Machine Learning and Medical Engineering for Cardiovascular Health and Intravascular Imaging and Computer Assisted Stenting*. Cham, Switzerland: Springer, 2019, pp. 158–166.

[101] J. Wei, Y. Xia, and Y. Zhang, "M3Net: A multi-model, multi-size, and multi-view deep neural network for brain magnetic resonance image segmentation," *Pattern Recognit.*, vol. 91, pp. 366–378, Jul. 2019.

[102] S. Minaee, Y. Boykov, F. Porikli, A. Plaza, N. Kehtarnavaz, and D. Terzopoulos, "Image segmentation using deep learning: A survey," Apr. 2020, *arXiv:2001.05566*. Accessed: Jun. 08, 2020. [Online]. Available: http://arxiv.org/abs/2001.05566

[103] V. Badrinarayanan, A. Kendall, and R. Cipolla, "SegNet: A deep convolutional encoder-decoder architecture for image segmentation," *IEEE Trans. Pattern Anal. Mach. Intell.*, vol. 39, no. 12, pp. 2481–2495, Dec. 2017.

[104] T.-Y. Lin, P. Dollár, R. Girshick, K. He, B. Hariharan, and S. Belongie, "Feature pyramid networks for object detection," in *Proc. IEEE Conf. Comput. Vis. Pattern Recognit. (CVPR)*, Jul. 2017, pp. 2117–2125.

[105] S. Seferbekov, V. Iglovikov, A. Buslaev, and A. Shvets, "Feature pyramid network for multi-class land segmentation," in *Proc. IEEE Conf. Comput. Vis. Pattern Recognit. (CVPR) Workshops*, Jun. 2018, pp. 272–275.

[106] L.-C. Chen, G. Papandreou, I. Kokkinos, K. Murphy, and A. L. Yuille, "DeepLab: Semantic image segmentation with deep convolutional nets, atrous convolution, and fully connected CRFs," *IEEE Trans. Pattern Anal. Mach. Intell.*, vol. 40, no. 4, pp. 834–848, Apr. 2018.

[107] Q. Jin, Z. Meng, T. D. Pham, Q. Chen, L. Wei, and R. Su, "DUNet: A deformable network for retinal vessel segmentation," *Knowl.-Based Syst.*, vol. 178, pp. 149–162, Aug. 2019, doi: 10.1016/j.knosys.2019.04.025.

[108] S. M. Kamrul Hasan and C. A. Linte, "A modified U-Net convolutional network featuring a nearest-neighbor re-sampling-based elastic-transformation for brain tissue characterization and segmentation," in *Proc. IEEE Western New York Image Signal Process. Workshop (WNYISPW)*, Oct. 2018, pp. 1–5.

[109] S. Li, G. K. F. Tso, and K. He, "Bottleneck feature supervised U-Net for pixel-wise liver and tumor segmentation," *Expert Syst. Appl.*, vol. 145, May 2020, Art. no. 113131.

[110] A. Colonna, F. Scarpa, and A. Ruggeri, "Segmentation of corneal nerves using a U-Net-based convolutional neural network," in *Computational Pathology and Ophthalmic Medical Image Analysis*. Cham, Switzerland: Springer, 2018, pp. 185–192.

[111] H. Dong, G. Yang, F. Liu, Y. Mo, and Y. Guo, "Automatic brain tumor detection and segmentation using U-Net based fully convolutional networks," in *Proc. Annu. Conf. Med. Image Understand. Anal.*, 2017, pp. 506–517.

[112] H. T. Le and H. T.-T. Pham, "Brain tumor segmentation using U-Net based deep neural networks," in *Proc. Int. Conf. Develop. Biomed. Eng. Vietnam*, 2018, pp. 39–42.

[113] A. Kermi, I. Mahmoudi, and M. T. Khadir, "Deep convolutional neural networks using U-Net for automatic brain tumor segmentation in multimodal MRI volumes," in *Proc. Int. MICCAI Brainlesion Workshop*, 2018, pp. 37–48.

[114] S. Chen, C. Ding, and M. Liu, "Dual-force convolutional neural networks for accurate brain tumor segmentation," *Pattern Recognit.*, vol. 88, pp. 90–100, Apr. 2019.

[115] X. Kong, G. Sun, Q. Wu, J. Liu, and F. Lin, "Hybrid pyramid U-Net model for brain tumor segmentation," in *Proc. Int. Conf. Intell. Inf. Process.*, 2018, pp. 346–355.

[116] A. Bousselham, O. Bouattane, M. Youssfi, and A. Raihani, "Improved brain tumor segmentation in MRI images based on thermal analysis model using U-Net and GPUs," in *Proc. Int. Conf. Adv. Intell. Syst. Sustain. Develop.*, 2019, pp. 80–87.

[117] Y. Chen, Z. Cao, C. Cao, J. Yang, and J. Zhang, "A modified U-Net for brain MR image segmentation," in *Proc. Int. Conf. Cloud Comput. Secur.*, 2018, pp. 233–242.

[118] Z. Wu, F. Chen, and D. Wu, "A novel framework called HDU for segmentation of brain tumor," in *Proc. 15th Int. Comput. Conf. Wavelet Act. Media Technol. Inf. Process. (ICCWAMTIP)*, Dec. 2018, pp. 81–84.

[119] T. Yang and J. Song, "An automatic brain tumor image segmentation method based on the U-Net," in *Proc. IEEE 4th Int. Conf. Comput. Commun. (ICCC)*, Dec. 2018, pp. 1600–1604.

[120] J. Dutta, D. Chakraborty, and D. Mondal, "Multimodal segmentation of brain tumours in volumetric MRI scans of the brain using time-distributed U-Net," in *Computational Intelligence in Pattern Recognition*. Singapore: Springer, 2020, pp. 715–725.

[121] R. Mehta, T. Christinck, T. Nair, P. Lemaitre, D. Arnold, and T. Arbel, "Propagating uncertainty across cascaded medical imaging tasks for improved deep learning inference," in *Uncertainty for Safe Utilization of Machine Learning in Medical Imaging and Clinical Image-Based Procedures*. Cham, Switzerland: Springer, 2019, pp. 23–32.

[122] A. K. Dhara, K. R. Ayyalasomayajula, E. Arvids, M. Fahlström, J. Wikström, E.-M. Larsson, and R. Strand, "Segmentation of post-operative glioblastoma in MRI by U-Net with patient-specific interactive refinement," in *Proc. Int. MICCAI Brainlesion Workshop*, 2018, pp. 115–122.

[123] A. Rafi, J. Ali, T. Akram, K. Fiaz, A. R. Shahid, B. Raza, and T. M. Madni, "U-Net based glioblastoma segmentation with patient's overall survival prediction," in *Proc. Int. Symp. Intell. Comput. Syst.*, 2020, pp. 22–32.

[124] P. X. Nguyen, Z. Lu, W. Huang, S. Huang, A. Katsuki, and Z. Lin, "Medical image segmentation with stochastic aggregated loss in a unified U-Net," in *Proc. IEEE EMBS Int. Conf. Biomed. Health Informat. (BHI)*, May 2019, pp. 1–4.

[125] Y. Xu, M. Gong, H. Fu, D. Tao, K. Zhang, and K. Batmanghelich, "Multi-scale masked 3-D U-Net for brain tumor segmentation," in *Proc. Int. MICCAI Brainlesion Workshop*, 2018, pp. 222–233.

[126] K. M. B. Dev, P. S. Jogi, S. Niyas, S. Vinayagamani, C. Kesavadas, and J. Rajan, "Automatic detection and localization of focal cortical dysplasia lesions in MRI using fully convolutional neural network," *Biomed. Signal Process. Control*, vol. 52, pp. 218–225, Jul. 2019.

[127] A. Zaman, L. Zhang, J. Yan, and D. Zhu, "Multi-modal image prediction via spatial hybrid U-Net," in *Proc. Int. Workshop Multiscale Multimodal Med. Imag.*, 2019, pp. 1–9.

[128] M. Jafari, R. Li, Y. Xing, D. Auer, S. Francis, J. Garibaldi, and X. Chen, "FU-Net: Multi-class image segmentation using feedback weighted U-Net," in *Proc. Int. Conf. Image Graph.*, 2019, pp. 529–537.

[129] W. Yao, S. Wang, and H. Fu, "Hippocampus segmentation in MRI using side U-Net model," in *Proc. Int. Conf. Neural Inf. Process.*, 2019, pp. 143–150.

[130] Y. Zhang, W. Chen, Y. Chen, and X. Tang, "A post-processing method to improve the white matter hyperintensity segmentation accuracy for randomly-initialized U-Net," in *Proc. IEEE 23rd Int. Conf. Digit. Signal Process. (DSP)*, Nov. 2018, pp. 1–5.

[131] J. Wu, Y. Zhang, K. Wang, and X. Tang, "Skip connection U-Net for white matter hyperintensities segmentation from MRI," *IEEE Access*, vol. 7, pp. 155194–155202, 2019.

[132] Y. Zhang, J. Wu, W. Chen, Y. Liu, J. Lyu, H. Shi, Y. Chen, E. X. Wu, and X. Tang, "Fully automatic white matter hyperintensity segmentation using U-Net and skip connection," in *Proc. 41st Annu. Int. Conf. IEEE Eng. Med. Biol. Soc. (EMBC)*, Jul. 2019, pp. 974–977.

[133] S. S. M. Salehi, D. Erdogmus, and A. Gholipour, "Auto-context convolutional neural network (Auto-Net) for brain extraction in magnetic resonance imaging," *IEEE Trans. Med. Imag.*, vol. 36, no. 11, pp. 2319–2330, Nov. 2017.

[134] A. Rampun, D. Jarvis, P. Griffiths, and P. Armitage, "Automated 2D fetal brain segmentation of MR images using a deep U-Net," in *Proc. Asian Conf. Pattern Recognit.*, 2019, pp. 373–386.

[135] J. Lou, D. Li, T. D. Bui, F. Zhao, L. Sun, G. Li, and D. Shen, "Automatic fetal brain extraction using multi-stage U-Net with deep supervision," in *Proc. Int. Workshop Mach. Learn. Med. Imag.*, 2019, pp. 592–600.

[136] G. Wang, W. Li, M. A. Zuluaga, R. Pratt, P. A. Patel, M. Aertsen, T. Doel, A. L. David, J. Deprest, S. Ourselin, and T. Vercauteren, "Interactive medical image segmentation using deep learning with image-specific fine tuning," *IEEE Trans. Med. Imag.*, vol. 37, no. 7, pp. 1562–1573, Jul. 2018.

[137] G. R. Pinheiro, R. Voltoline, M. Bento, and L. Rittner, "V-Net and U-Net for ischemic stroke lesion segmentation in a small dataset of perfusion data," in *Proc. Int. MICCAI Brainlesion Workshop*, 2018, pp. 301–309.

[138] R. Karthik, U. Gupta, A. Jha, R. Rajalakshmi, and R. Menaka, "A deep supervised approach for ischemic lesion segmentation from multimodal MRI using fully convolutional network," *Appl. Soft Comput.*, vol. 84, Nov. 2019, Art. no. 105685.

[139] A. Bousselham, O. Bouattane, M. Youssfi, and A. Raihani, "Ischemic stroke lesion segmentation based on thermal analysis model using U-Net fully convolutional neural networks on GPUs," in *Proc. Int. Conf. Adv. Intell. Syst. Sustain. Develop.*, 2019, pp. 99–106.

[140] L. K. S. Cornelio, M. A. V. del Castillo, and P. C. Naval, Jr., "U-ISLES: Ischemic stroke lesion segmentation using U-Net," in *Proc. SAI Intell. Syst. Conf.*, 2018, pp. 326–336.

[141] J. Kobold, E. Lang, A. M. Tome, V. Vigneron, H. Maaref, D. Fourer, M. Aghasaryan, C. Alecu, N. Chausson, Y. L'Hermitte, and D. Smadja, "Stroke thrombus segmentation on SWAN with multi-directional U-Nets," in *Proc. 9th Int. Conf. Image Process. Theory, Tools Appl. (IPTA)*, Nov. 2019, pp. 1–6.

[142] H. Yang, Z. Liu, and X. Yang, "Right ventricle segmentation in short-axis MRI using a shape constrained dense connected U-Net," in *Proc. Int. Conf. Med. Image Comput. Comput.-Assist. Intervent.*, 2019, pp. 532–540.

[143] Y.-C. Kim, K. R. Kim, and Y. H. Choe, "Automatic myocardial segmentation in dynamic contrast enhanced perfusion MRI using Monte Carlo dropout in an encoder-decoder convolutional neural network," *Comput. Methods Programs Biomed.*, vol. 185, Mar. 2020, Art. no. 105150.

[144] W. Yan, Y. Wang, Z. Li, R. J. Van Der Geest, and Q. Tao, "Left ventricle segmentation via optical-flow-net from short-axis cine MRI: Preserving the temporal coherence of cardiac motion," in *Proc. Int. Conf. Med. Image Comput. Comput.-Assist. Intervent.*, 2018, pp. 613–621.

[145] J. Zhang, J. Du, H. Liu, X. Hou, Y. Zhao, and M. Ding, "LU-NET: An improved U-Net for ventricular segmentation," *IEEE Access*, vol. 7, pp. 92539–92546, 2019.

[146] S. Charmchi, K. Punithakumar, and P. Boulanger, "Optimizing U-Net to segment left ventricle from magnetic resonance imaging," in *Proc. IEEE Int. Conf. Bioinf. Biomed. (BIBM)*, Dec. 2018, pp. 327–332.

[147] G. Borodin and O. Senyukova, "Right ventricle segmentation in cardiac MR images using U-Net with partly dilated convolution," in *Proc. Int. Conf. Artif. Neural Netw.*, 2018, pp. 179–185.

[148] X. Wang, S. Yang, M. Tang, Y. Wei, X. Han, L. He, and J. Zhang, "SK-Unet: An improved U-Net model with selective kernel for the segmentation of multi-sequence cardiac MR," in *Proc. Int. Workshop Stat. Atlases Comput. Models Heart*, 2019, pp. 246–253.

[149] X.-Y. Zhou, P. Li, Z.-Y. Wang, and G.-Z. Yang, "U-Net training with instance-layer normalization," in *Proc. Int. Workshop Multiscale Multimodal Med. Imag.*, 2019, pp. 101–108.

[150] W. Yan, Y. Wang, R. J. van der Geest, and Q. Tao, "Cine MRI analysis by deep learning of optical flow: Adding the temporal dimension," *Comput. Biol. Med.*, vol. 111, Aug. 2019, Art. no. 103356.

[151] F. Guo, M. Ng, and G. Wright, "Cardiac MRI left ventricle segmentation and quantification: A framework combining U-Net and continuous max-flow," in *Proc. Int. Workshop Stat. Atlases Comput. Models Heart*, 2018, pp. 450–458.

[152] R. J. Nowling, J. Bukowy, S. D. McGarry, A. S. Nencka, O. Blasko, J. Urbain, A. Lowman, A. Barrington, A. Banerjee, K. A. Iczkowski, and P. S. LaViolette, "Classification before segmentation: Improved U-Net prostate segmentation," in *Proc. IEEE EMBS Int. Conf. Biomed. Health Informat. (BHI)*, May 2019, pp. 1–4.

[153] Y. Zhang, J. Wu, W. Chen, Y. Chen, and X. Tang, "Prostate segmentation using Z-Net," in *Proc. IEEE 16th Int. Symp. Biomed. Imag. (ISBI)*, Apr. 2019, pp. 11–14.

[154] L. Rundo, C. Han, Y. Nagano, J. Zhang, R. Hataya, C. Militello, A. Tangherloni, M. S. Nobile, C. Ferretti, D. Besozzi, M. C. Gilardi, S. Vitabile, G. Mauri, H. Nakayama, and P. Cazzaniga, "USE-Net: Incorporating squeeze-and-excitation blocks into U-Net for prostate zonal segmentation of multi-institutional MRI datasets," *Neurocomputing*, vol. 365, pp. 31–43, Nov. 2019.

[155] S. Elguindi, M. J. Zelefsky, J. Jiang, H. Veeraraghavan, J. O. Deasy, M. A. Hunt, and N. Tyagi, "Deep learning-based auto-segmentation of targets and organs-at-risk for magnetic resonance imaging only planning of prostate radiotherapy," *Phys. Imag. Radiat. Oncol.*, vol. 12, pp. 80–86, Oct. 2019.

[156] Y. Weng, T. Zhou, Y. Li, and X. Qiu, "NAS-UNet: Neural architecture search for medical image segmentation," *IEEE Access*, vol. 7, pp. 44247–44257, 2019.

[157] A. Fabijańska, A. Vacavant, M.-A. Lebre, A. L. M. Pavan, D. R. de Pina, A. Abergel, P. Chabrot, and B. Magnin, "U-CatcHCC: An accurate HCC detector in hepatic DCE-MRI sequences based on an U-Net framework," in *Proc. Int. Conf. Comput. Vis. Graph.*, 2018, pp. 319–328.

[158] Y. Wang, Y. Song, F. Wang, J. Sun, X. Gao, Z. Han, L. Shi, G. Shao, M. Fan, and G. Yang, "A two-step automated quality assessment for liver MR images based on convolutional neural network," *Eur. J. Radiol.*, vol. 124, Mar. 2020, Art. no. 108822.

[159] B. Zhao, J. Soraghan, G. D. Caterina, and D. Grose, "Segmentation of head and neck tumours using modified U-Net," in *Proc. 27th Eur. Signal Process. Conf. (EUSIPCO)*, Sep. 2019, pp. 1–4.

[160] G. Piantadosi, S. Marrone, A. Galli, M. Sansone, and C. Sansone, "DCE-MRI breast lesions segmentation with a 3TP U-Net deep convolutional neural network," in *Proc. IEEE 32nd Int. Symp. Comput.-Based Med. Syst. (CBMS)*, Jun. 2019, pp. 628–633.

[161] M. AskariHemmat, S. Honari, L. Rouhier, C. S. Perone, J. Cohen-Adad, Y. Savaria, and J.-P. David, "U-Net fixed-point quantization for medical image segmentation," in *Large-Scale Annotation of Biomedical Data and Expert Label Synthesis and Hardware Aware Learning for Medical Imaging and Computer Assisted Intervention*. Cham, Switzerland: Springer, 2019, pp. 115–124.

[162] F. Paugam, J. Lefeuvre, C. S. Perone, C. Gros, D. S. Reich, P. Sati, and J. Cohen-Adad, "Open-source pipeline for multi-class segmentation of the spinal cord with deep learning," *Magn. Reson. Imag.*, vol. 64, pp. 21–27, Dec. 2019.

[163] M. Han, Y. Bao, Z. Sun, S. Wen, L. Xia, J. Zhao, J. Du, and Z. Yan, "Automatic segmentation of human placenta images with U-Net," *IEEE Access*, vol. 7, pp. 180083–180092, 2019.

[164] Y. Kurata, M. Nishio, A. Kido, K. Fujimoto, M. Yakami, H. Isoda, and K. Togashi, "Automatic segmentation of the uterus on MRI using a convolutional neural network," *Comput. Biol. Med.*, vol. 114, Nov. 2019, Art. no. 103438.

[165] V. Garg, M. Bansal, A. Sanjana, and M. Dave, "Analysis and detection of brain tumor using U-Net-based deep learning," in *Proc. Sci. Inf. Conf.*, Jul. 2020, pp. 161–173, doi: 10.1007/978-3-030-52243-8_13.

[166] H. M. Rai and K. Chatterjee, "Detection of brain abnormality by a novel Lu-Net deep neural CNN model from MR images," *Mach. Learn. Appl.*, vol. 2, Dec. 2020, Art. no. 100004, doi: 10.1016/j.mlwa.2020.100004.

[167] S. E. I. El Kaitouni and H. Tairi, "Segmentation of medical images for the extraction of brain tumors: A comparative study between the hidden Markov and deep learning approaches," in *Proc. Int. Conf. Intell. Syst. Comput. Vis. (ISCV)*, Jun. 2020, pp. 1–5, doi: 10.1109/ISCV49265.2020.9204319.

[168] Z. Wang and L. Zhang, "Semantic segmentation of brain MRI based on U-Net network and edge loss," in *Proc. 19th Int. Symp. Distrib. Comput. Appl. Bus. Eng. Sci. (DCABES)*, Oct. 2020, pp. 154–157, doi: 10.1109/DCABES50732.2020.00048.

[169] M. A. Ahamed, M. Ali Hossain, and M. Al Mamun, "Semantic segmentation of self-supervised dataset and medical images using combination of U-Net and neural ordinary differential equations," in *Proc. IEEE Region Symp. (TENSYMP)*, Jun. 2020, pp. 238–241, doi: 10.1109/TENSYMP50017.2020.9230884.

[170] S. Subramaniam, K. B. Jayanthi, C. Rajasekaran, and R. Kuchelar, "Deep learning architectures for medical image segmentation," in *Proc. IEEE 33rd Int. Symp. Comput.-Based Med. Syst. (CBMS)*, Jul. 2020, pp. 579–584, doi: 10.1109/CBMS49503.2020.00115.

[171] A. Mehrtash, W. M. Wells, C. M. Tempany, P. Abolmaesumi, and T. Kapur, "Confidence calibration and predictive uncertainty estimation for deep medical image segmentation," *IEEE Trans. Med. Imag.*, vol. 39, no. 12, pp. 3868–3878, Jul. 2020, doi: 10.1109/TMI.2020.3006437.

[172] Z. Ji, X. Han, T. Lin, and W. Wang, "A dense-gated U-Net for brain lesion segmentation," in *Proc. IEEE Int. Conf. Vis. Commun. Image Process. (VCIP)*, Dec. 2020, pp. 104–107, doi: 10.1109/VCIP49819.2020.9301852.

[173] W. Shi, E. Pang, Q. Wu, and F. Lin, "Brain tumor segmentation using dense channels 2D U-Net and multiple feature extraction network," in *Proc. Int. MICCAI Brainlesion Workshop*, Oct. 2019, pp. 273–283, doi: 10.1007/978-3-030-46640-4_26.

[174] R. Yogesh, N. Malarvizhi, and G. Sasi, "Narcotic image segmentation utilizing MR U-Net design," in *Proc. Int. Conf. Syst., Comput., Automat. Netw. (ICSCAN)*, Jul. 2020, pp. 1–6, doi: 10.1109/ICSCAN49426.2020.9262362.

[175] N. Micallef, D. Seychell, and C. J. Bajada, "A nested U-Net approach for brain tumour segmentation," in *Proc. IEEE 20th Medit. Electrotechn. Conf. (MELECON)*, Jun. 2020, pp. 376–381, doi: 10.1109/MELECON48756.2020.9140550.

[176] M. Jafari, D. Auer, S. Francis, J. Garibaldi, and X. Chen, "DRU-Net: An efficient deep convolutional neural network for medical image segmentation," in *Proc. IEEE 17th Int. Symp. Biomed. Imag. (ISBI)*, Apr. 2020, pp. 1144–1148, doi: 10.1109/ISBI45749.2020.9098391.

[177] S. Chen, G. Hu, and J. Sun, "Medical image segmentation based on 3D U-Net," in *Proc. 19th Int. Symp. Distrib. Comput. Appl. Bus. Eng. Sci. (DCABES)*, Oct. 2020, pp. 130–133, doi: 10.1109/DCABES50732.2020.00042.

[178] T. Jesus, R. Magalhães, and V. Alves, "Spatial normalization of MRI brain studies using a U-Net based neural network," in *Proc. World Conf. Inf. Syst. Technol.*, Apr. 2020, pp. 493–502, doi: 10.1007/978-3-030-45697-9_48.

[179] K. Ryu, N.-Y. Shin, D.-H. Kim, and Y. Nam, "Synthesizing t1 weighted MPRAGE image from multi echo GRE images via deep neural network," *Magn. Reson. Imag.*, vol. 64, pp. 13–20, Dec. 2019.

[180] L. Zhao, X. Feng, C. H. Meyer, and D. C. Alsop, "Choroid plexus segmentation using optimized 3D U-Net," in *Proc. IEEE 17th Int. Symp. Biomed. Imag. (ISBI)*, Apr. 2020, pp. 381–384, doi: 10.1109/ISBI45749.2020.9098443.

[181] D. Ai, Z. Zhao, J. Fan, H. Song, X. Qu, J. Xian, and J. Yang, "Spatial probabilistic distribution map-based two-channel 3D U-Net for visual pathway segmentation," *Pattern Recognit. Lett.*, vol. 138, pp. 601–607, Oct. 2020, doi: 10.1016/j.patrec.2020.09.003.

[182] B. E. Dewey, C. Zhao, J. C. Reinhold, A. Carass, K. C. Fitzgerald, E. S. Sotirchos, S. Saidha, J. Oh, D. L. Pham, P. A. Calabresi, P. C. M. van Zijl, and J. L. Prince, "DeepHarmony: A deep learning approach to contrast harmonization across scanner changes," *Magn. Reson. Imag.*, vol. 64, pp. 160–170, Dec. 2019.

[183] M. Zhao, Y. Wei, Y. Lu, and K. K. L. Wong, "A novel U-Net approach to segment the cardiac chamber in magnetic resonance images with ghost artifacts," *Comput. Methods Programs Biomed.*, vol. 196, Nov. 2020, Art. no. 105623, doi: 10.1016/j.cmpb.2020.105623.

[184] B. Wu, Y. Fang, and X. Lai, "Left ventricle automatic segmentation in cardiac MRI using a combined CNN and U-Net approach," *Comput. Med. Imag. Graph.*, vol. 82, Jun. 2020, Art. no. 101719, doi: 10.1016/j.compmedimag.2020.101719.

[185] A. Elif and O. Ilkay, "Accurate myocardial pathology segmentation with residual U-Net," in *Proc. Myocardial Pathol. Segmentation Combining Multi-Sequence CMR Challenge*, Jan. 2020, pp. 128–137.

[186] H. Yu, S. Zha, Y. Huangfu, C. Chen, M. Ding, and J. Li, "Dual attention U-Net for multi-sequence cardiac MR images segmentation," in *Proc. Myocardial Pathol. Segmentation Combining Multi-Sequence CMR Challenge*, Jan. 2020, pp. 118–127.

[187] M. B. Calisto and S. K. Lai-Yuen, "AdaEn-Net: An ensemble of adaptive 2D-3D fully convolutional networks for medical image segmentation," *Neural Netw.*, vol. 126, pp. 76–94, Jun. 2020, doi: 10.1016/j.neunet.2020.03.007.

[188] B. Murugesan, K. Sarveswaran, V. S. Raghavan, S. M. Shankaranarayana, K. Ram, and M. Sivaprakasam, "A context based deep learning approach for unbalanced medical image segmentation," in *Proc. IEEE 17th Int. Symp. Biomed. Imag. (ISBI)*, Apr. 2020, pp. 1949–1953, doi: 10.1109/ISBI45749.2020.9098597.

[189] J. Sun, F. Darbehani, M. Zaidi, and B. Wang, "SAUNet: Shape attentive U-Net for interpretable medical image segmentation," in *Proc. Int. Conf. Med. Image Comput. Comput.-Assist. Intervent.*, Oct. 2020, pp. 797–806, doi: 10.1007/978-3-030-59719-1_77.

[190] S. Dong, J. Zhao, M. Zhang, Z. Shi, J. Deng, Y. Shi, M. Tian, and C. Zhuo, "DeU-Net: Deformable U-Net for 3D cardiac MRI video segmentation," in *Proc. Int. Conf. Med. Image Comput. Comput.-Assist. Intervent.*, Oct. 2020, pp. 98–107, doi: 10.1007/978-3-030-59719-1_10.

[191] P. Hambarde, S. Talbar, A. Mahajan, S. Chavan, M. Thakur, and N. Sable, "Prostate lesion segmentation in MR images using radiomics based deeply supervised U-Net," *Biocybern. Biomed. Eng.*, vol. 40, no. 4, pp. 1421–1435, Oct. 2020, doi: 10.1016/j.bbe.2020.07.011.

[192] A. Machireddy, N. Meermeier, F. Coakley, and X. Song, "Malignancy detection in prostate multi-parametric MR images using U-Net with attention," in *Proc. 42nd Annu. Int. Conf. IEEE Eng. Med. Biol. Soc. (EMBC)*, Jul. 2020, pp. 1520–1523, doi: 10.1109/EMBC44109.2020.9176050.

[193] C. Li, Y. Tan, W. Chen, X. Luo, Y. He, Y. Gao, and F. Li, "ANU-Net: Attention-based nested U-Net to exploit full resolution features for medical image segmentation," *Comput. Graph.*, vol. 90, pp. 11–20, Aug. 2020, doi: 10.1016/j.cag.2020.05.003.

[194] Z. Liu, Y.-Q. Song, V. S. Sheng, L. Wang, R. Jiang, X. Zhang, and D. Yuan, "Liver CT sequence segmentation based with improved U-Net and graph cut," *Expert Syst. Appl.*, vol. 126, pp. 54–63, Jul. 2019.

[195] B. Sakboonyara and P. Taeprasartsit, "U-Net and mean-shift histogram for efficient liver segmentation from CT images," in *Proc. 11th Int. Conf. Knowl. Smart Technol. (KST)*, Jan. 2019, pp. 51–56.

[196] T.-Y. Su and Y.-H. Fang, "Automatic liver and spleen segmentation with CT images using multi-channel U-Net deep learning approach," in *Proc. Int. Conf. Biomed. Health Informat.*, 2019, pp. 33–41.

[197] B. A. Skourt, A. El Hassani, and A. Majda, "Lung CT image segmentation using deep neural networks," *Procedia Comput. Sci.*, vol. 127, pp. 109–113, Jan. 2018.

[198] W. Tan, Y. Liu, H. Liu, J. Yang, X. Yin, and Y. Zhang, "A segmentation method of lung parenchyma from chest CT images based on dual U-Net," in *Proc. IEEE Int. Conf. Bioinf. Biomed. (BIBM)*, Nov. 2019, pp. 1649–1656.

[199] H. Shaziya, K. Shyamala, and R. Zaheer, "Automatic lung segmentation on thoracic CT scans using U-Net convolutional network," in *Proc. Int. Conf. Commun. Signal Process. (ICCSP)*, Apr. 2018, pp. 0643–0647.

[200] G. Tong, Y. Li, H. Chen, Q. Zhang, and H. Jiang, "Improved U-Net network for pulmonary nodules segmentation," *Optik*, vol. 174, pp. 460–469, Dec. 2018.

[201] Z. Gu, J. Cheng, H. Fu, K. Zhou, H. Hao, Y. Zhao, T. Zhang, S. Gao, and J. Liu, "CE-Net: Context encoder network for 2D medical image segmentation," *IEEE Trans. Med. Imag.*, vol. 38, no. 10, pp. 2281–2292, Oct. 2019.

[202] Z. Liu, X. Liu, B. Xiao, S. Wang, Z. Miao, Y. Sun, and F. Zhang, "Segmentation of organs-at-risk in cervical cancer CT images with a convolutional neural network," *Phys. Medica*, vol. 69, pp. 184–191, Jan. 2020.

[203] N. Yagi, M. Nii, and S. Kobashi, "Abdominal organ area segmentation using U-Net for cancer radiotherapy support," in *Proc. IEEE Int. Conf. Syst., Man Cybern. (SMC)*, Oct. 2019, pp. 1210–1214.

[204] C. Wang, B. Connolly, P. F. de Oliveira Lopes, A. F. Frangi, and Ö. Smedby, "Pelvis segmentation using multi-pass U-Net and iterative shape estimation," in *Proc. Int. Workshop Comput. Methods Clin. Appl. Musculoskeletal Imag.*, 2018, pp. 49–57.

[205] H. Seo, C. Huang, M. Bassenne, R. Xiao, and L. Xing, "Modified U-Net (mU-Net) with incorporation of object-dependent high level features for improved liver and liver-tumor segmentation in CT images," *IEEE Trans. Med. Imag.*, vol. 39, no. 5, pp. 1316–1325, May 2020, doi: 10.1109/TMI.2019.2948320.

[206] Y.-C. Liu, M. Shahid, W. Sarapugdi, Y.-X. Lin, J.-C. Chen, and K.-L. Hua, "Cascaded atrous dual attention U-Net for tumor segmentation," *Multimedia Tools Appl.*, Oct. 2020, doi: 10.1007/S11042-020-10078-2.

[207] S. Li, G. K. F. Tso, and K. He, "Bottleneck feature supervised U-Net for pixel-wise liver and tumor segmentation," *Expert Syst. Appl.*, vol. 145, May 2020, Art. no. 113131, doi: 10.1016/j.eswa.2019.113131.

[208] J. Rocha, A. Cunha, and A. M. Mendonça, "Conventional filtering versus U-Net based models for pulmonary nodule segmentation in CT images," *J. Med. Syst.*, vol. 44, no. 4, p. 81, Mar. 2020, doi: 10.1007/S10916-020-1541-9.

[209] K. Suzuki, Y. Otsuka, Y. Nomura, K. K. Kumamaru, R. Kuwatsuru, and S. Aoki, "Development and validation of a modified three-dimensional U-Net deep-learning model for automated detection of lung nodules on chest CT images from the lung image database consortium and Japanese datasets," *Academic Radiol.*, Aug. 2020, doi: 10.1016/j.acra.2020.07.030.

[210] K. Yang, J. Liu, W. Tang, H. Zhang, R. Zhang, J. Gu, R. Zhu, J. Xiong, X. Ru, and J. Wu, "Identification of benign and malignant pulmonary nodules on chest CT using improved 3D U-Net deep learning framework," *Eur. J. Radiol.*, vol. 129, Aug. 2020, Art. no. 109013, doi: 10.1016/j.ejrad.2020.109013.

[211] A. Khanna, N. D. Londhe, S. Gupta, and A. Semwal, "A deep residual U-Net convolutional neural network for automated lung segmentation in computed tomography images," *Biocybern. Biomed. Eng.*, vol. 40, no. 3, pp. 1314–1327, Jul. 2020, doi: 10.1016/j.bbe.2020.07.007.

[212] Y. Zhou, M. Chen, M. Zhang, T. Wang, F. Yan, and C. Xie, "Automatic segmentation of lung noudles using improved U-Net NetWork," in *Proc. Chin. Automat. Congr. (CAC)*, Nov. 2020, pp. 1609–1613, doi: 10.1109/CAC51589.2020.9326834.

[213] C. Wang, Z. Wang, W. Xi, Z. Yang, G. Bai, R. Wang, and M. Duan, "MufiNet: Multiscale fusion residual networks for medical image segmentation," in *Proc. Int. Joint Conf. Neural Netw. (IJCNN)*, Jul. 2020, pp. 1–7, doi: 10.1109/IJCNN48605.2020.9207314.

[214] A. G. Rassadin, "Deep residual 3D U-Net for joint segmentation and texture classification of nodules in lung," in *Proc. Int. Conf. Image Anal. Recognit.*, Jun. 2020, pp. 419–427, doi: 10.1007/978-3-030-50516-5_37.

[215] W. Ying, J. Li, Y. Wu, K. Zheng, Y. Deng, and J. Li, "U-Net with dense encoder, residual decoder and depth-wise skip connections," in *Proc. Int. Joint Conf. Neural Netw. (IJCNN)*, Jul. 2020, pp. 1–6, doi: 10.1109/IJCNN48605.2020.9207371.

[216] A. Kumar, S. Agarwala, A. K. Dhara, D. Nandi, S. B. Thakur, A. K. Bhadra, and A. Sadhu, "Segmentation of lung field in HRCT images using U-Net based fully convolutional networks," in *Proc. Annu. Conf. Med. Image Understand. Anal.*, 2018, pp. 84–93.

[217] S. Hernández-Juárez, A. R. Mejía-Rodríguez, E. R. Arce-Santana, S. Charleston-Villalobos, A. T. Aljama-Corrales, R. González-Camarena, and M. Mejía-Ávila, "Semantic segmentation of lung tissues in HRCT images by means of a U-Net convolutional network," in *Proc. Latin Amer. Conf. Biomed. Eng.*, 2019, pp. 426–434.

[218] A. Yang, X. Jin, and L. Li, "CT images recognition of pulmonary tuberculosis based on improved faster RCNN and U-Net," in *Proc. 10th Int. Conf. Inf. Technol. Med. Educ. (ITME)*, Aug. 2019, pp. 93–97.

[219] M. O. Ramkumar, D. Jayakumar, and R. Yogesh, "Multi res U-Net based image segmentation of pulmonary tuberculosis using CT images," in *Proc. 7th Int. Conf. Smart Struct. Syst. (ICSSS)*, Jul. 2020, pp. 1–4, doi: 10.1109/ICSSS49621.2020.9202371.

[220] E. Kurnaz and R. Ceylan, "Pancreas segmentation in abdominal CT images with U-Net model," in *Proc. 28th Signal Process. Commun. Appl. Conf. (SIU)*, Oct. 2020, pp. 1–4, doi: 10.1109/SIU49456.2020.9302180.

[221] X. Ding, Y. Peng, C. Shen, and T. Zeng, "CAB U-Net: An end-to-end category attention boosting algorithm for segmentation," *Comput. Med. Imag. Graph.*, vol. 84, Sep. 2020, Art. no. 101764, doi: 10.1016/j.compmedimag.2020.101764.

[222] Z. Lou, W. Huo, K. Le, and X. Tian, "Whole heart auto segmentation of cardiac CT images using U-Net based GAN," in *Proc. 13th Int. Congr. Image Signal Process., Biomed. Eng. Informat. (CISP-BMEI)*, Oct. 2020, pp. 192–196, doi: 10.1109/CISP-BMEI51763.2020.9263532.

[223] Y. Man, Y. Huang, J. Feng, X. Li, and F. Wu, "Deep Q learning driven CT pancreas segmentation with geometry-aware U-Net," *IEEE Trans. Med. Imag.*, vol. 38, no. 8, pp. 1971–1980, Aug. 2019.

[224] L. Wang, B. Wang, and Z. Xu, "Tumor segmentation based on deeply supervised multi-scale U-Net," in *Proc. IEEE Int. Conf. Bioinf. Biomed. (BIBM)*, Nov. 2019, pp. 746–749.

[225] A. Manvel, K. Vladimir, T. Alexander, and U. Dmitry, "Radiologist-level stroke classification on non-contrast CT scans with deep U-Net," in *Proc. Int. Conf. Med. Image Comput. Comput.-Assist. Intervent.*, 2019, pp. 820–828.

[226] D. Zhang, J. Wang, J. H. Noble, and B. M. Dawant, "HeadLoc-Net: Deep convolutional neural networks for accurate classification and multi-landmark localization of head CTs," *Med. Image Anal.*, vol. 61, Apr. 2020, Art. no. 101659.

[227] T. Song, F. Meng, A. Rodríguez-Patón, P. Li, P. Zheng, and X. Wang, "U-next: A novel convolution neural network with an aggregation U-Net architecture for gallstone segmentation in CT images," *IEEE Access*, vol. 7, pp. 166823–166832, 2019.

[228] W. Zhao, D. Jiang, J. Peña Queralta, and T. Westerlund, "MSS U-Net: 3D segmentation of kidneys and tumors from CT images with a multi-scale supervised U-Net," *Informat. Med. Unlocked*, vol. 19, Jan. 2020, Art. no. 100357, doi: 10.1016/j.imu.2020.100357.

[229] Z. Li, J. Pan, H. Wu, Z. Wen, and J. Qin, "Memory-efficient automatic kidney and tumor segmentation based on non-local context guided 3D U-Net," in *Proc. Int. Conf. Med. Image Comput. Comput.-Assist. Intervent.*, Oct. 2020, pp. 197–206, doi: 10.1007/978-3-030-59719-1_20.

[230] J. Chen, A. Cao, Y. Zhang, and T. Xu, "Tumor-assisted diagnosis based on U-Net network," in *Proc. 13th Int. Congr. Image Signal Process., Biomed. Eng. Informat. (CISP-BMEI)*, Oct. 2020, pp. 739–742, doi: 10.1109/CISP-BMEI51763.2020.9263550.

[231] X. Xu, C. Lian, S. Wang, A. Wang, T. Royce, R. Chen, J. Lian, and D. Shen, "Asymmetrical multi-task attention U-Net for the segmentation of prostate bed in CT image," in *Proc. Int. Conf. Med. Image Comput. Comput.-Assist. Intervent.*, Oct. 2020, pp. 470–479, doi: 10.1007/978-3-030-59719-1_46.

[232] J. Ni, J. Wu, J. Tong, Z. Chen, and J. Zhao, "GC-Net: Global context network for medical image segmentation," *Comput. Methods Programs Biomed.*, vol. 190, Jul. 2020, Art. no. 105121, doi: 10.1016/j.cmpb.2019.105121.

[233] L. Bargsten, M. Wendebourg, and A. Schlaefer, "Data representations for segmentation of vascular structures using convolutional neural networks with U-Net architecture," in *Proc. 41st Annu. Int. Conf. IEEE Eng. Med. Biol. Soc. (EMBC)*, Jul. 2019, pp. 989–992.

[234] G. Cao, Y. Wang, X. Zhu, M. Li, X. Wang, and Y. Chen, "Segmentation of intracerebral hemorrhage based on improved U-Net," in *Proc. IEEE Conf. Telecommun., Opt. Comput. Sci. (TOCS)*, Dec. 2020, pp. 183–185, doi: 10.1109/TOCS50858.2020.9339707.

[235] Z. Kuang, X. Deng, L. Yu, H. Wang, T. Li, and S. Wang, "Ψ-Net: Focusing on the border areas of intracerebral hemorrhage on CT images," *Comput. Methods Programs Biomed.*, vol. 194, Oct. 2020, Art. no. 105546, doi: 10.1016/j.cmpb.2020.105546.

[236] Y. Zhang, B. Lei, C. Fu, J. Du, X. Zhu, X. Han, L. Du, W. Gao, T. Wang, and G. Ma, "HBNet: Hybrid blocks network for segmentation of gastric tumor from ordinary CT images," in *Proc. IEEE 17th Int. Symp. Biomed. Imag. (ISBI)*, Apr. 2020, pp. 1–4, doi: 10.1109/ISBI45749.2020.9098425.

[237] G. Sha, J. Wu, and B. Yu, "Spinal fracture lesions segmentation based on U-Net," in *Proc. IEEE Int. Conf. Artif. Intell. Comput. Appl. (ICAICA)*, Jun. 2020, pp. 142–144, doi: 10.1109/ICAICA50127.2020.9182574.

[238] Y. Hiasa, Y. Otake, M. Takao, T. Ogawa, N. Sugano, and Y. Sato, "Automated muscle segmentation from clinical CT using Bayesian U-Net for personalized musculoskeletal modeling," *IEEE Trans. Med. Imag.*, vol. 39, no. 4, pp. 1030–1040, Apr. 2020, doi: 10.1109/TMI.2019.2940555.

[239] L. Luo, D. Chen, and D. Xue, "Retinal blood vessels semantic segmentation method based on modified U-Net," in *Proc. Chin. Control Decis. Conf. (CCDC)*, Jun. 2018, pp. 1892–1895, doi: 10.1109/CCDC.2018.8407435.

[240] J. Devda and R. Eswari, "Pathological myopia image analysis using deep learning," in *Proc. 2nd Int. Conf. Recent Trends Adv. Comput. ICRTAC-DISRUP-TIV Innov.*, vol. 165, Jan. 2019, pp. 239–244, doi: 10.1016/j.procs.2020.01.084.

[241] X. Xu, T. Tan, and F. Xu, "An improved U-Net architecture for simultaneous arteriole and venule segmentation in fundus image," in *Medical Image Understanding and Analysis*. Cham, Switzerland: Springer, 2018, pp. 333–340.

[242] W. Yijie, L. Shixuan, C. Guogang, C. Cong, L. Mengxue, and Z. Xinyu, "Improved U-Net fundus image segmentation method," in *Proc. Int. Conf. Intell. Informat. Biomed. Sci. (ICIIBMS)*, Nov. 2019, pp. 110–113, doi: 10.1109/ICIIBMS46890.2019.8991481.

[243] Z. Yan, X. Han, C. Wang, Y. Qiu, Z. Xiong, and S. Cui, "Learning mutually local-global U-Nets for high-resolution retinal lesion segmentation in fundus images," in *Proc. IEEE 16th Int. Symp. Biomed. Imag. (ISBI)*, Apr. 2019, pp. 597–600, doi: 10.1109/ISBI.2019.8759579.

[244] S. Kumawat and S. Raman, "Local phase U-Net for fundus image segmentation," in *Proc. IEEE Int. Conf. Acoust., Speech Signal Process. (ICASSP)*, May 2019, pp. 1209–1213, doi: 10.1109/ICASSP.2019.8683390.

[245] C. Guo, M. Szemenyei, Y. Pei, Y. Yi, and W. Zhou, "SD-UNet: A structured dropout U-Net for retinal vessel segmentation," in *Proc. IEEE 19th Int. Conf. Bioinf. Bioeng. (BIBE)*, Oct. 2019, pp. 439–444, doi: 10.1109/BIBE.2019.00085.

[246] S. Zhang, R. Zheng, Y. Luo, X. Wang, J. Mao, C. J. Roberts, and M. Sun, "Simultaneous arteriole and venule segmentation of dual-modal fundus images using a multi-task cascade network," *IEEE Access*, vol. 7, pp. 57561–57573, 2019, doi: 10.1109/ACCESS.2019.2914319.

[247] J. Civit-Masot, F. Luna-Perejón, S. Vicente-Díaz, J. M. R. Corral, and A. Civit, "TPU cloud-based generalized U-Net for eye fundus image segmentation," *IEEE Access*, vol. 7, pp. 142379–142387, 2019, doi: 10.1109/ACCESS.2019.2944692.

[248] A. Farahani and H. Mohseni, "Medical image segmentation using customized U-Net with adaptive activation functions," *Neural Comput. Appl.*, vol. 33, pp. 1–17, Oct. 2020, doi: 10.1007/S00521-020-05396-3.

[249] X.-M. Li, G.-S. Chen, and S.-Y. Wang, "Dense-atrous U-Net with salient computing for accurate retina vessel segmentation," in *Proc. IEEE 15th Int. Conf. Solid-State Integr. Circuit Technol. (ICSICT)*, Nov. 2020, pp. 1–3, doi: 10.1109/ICSICT49897.2020.9278165.

[250] E. S. Kumar and C. S. Bindu, "An efficient approach to accomplish automatic segmentation of optic cup using modified U-Net," in *Proc. 11th Int. Conf. Comput., Commun. Netw. Technol. (ICCCNT)*, Jul. 2020, pp. 1–5, doi: 10.1109/ICCCNT49239.2020.9225537.

[251] A. Desai, R. Chauhan, and J. Sivaswamy, "Image segmentation using hybrid representations," in *Proc. IEEE 17th Int. Symp. Biomed. Imag. (ISBI)*, Apr. 2020, pp. 1–4, doi: 10.1109/ISBI45749.2020.9098463.

[252] B. Wang, S. Qiu, and H. He, "Dual encoding U-Net for retinal vessel segmentation," in *Medical Image Computing and Computer Assisted Intervention*. Cham, Switzerland: Springer, 2019, pp. 84–92.

[253] Y. Li, Y. Wang, T. Leng, and W. Zhijie, "Wavelet U-Net for medical image segmentation," in *Proc. Int. Conf. Artif. Neural Netw.*, Sep. 2020, pp. 800–810, doi: 10.1007/978-3-030-61609-0_63.

[254] P. Xiuqin, Q. Zhang, H. Zhang, and S. Li, "A fundus retinal vessels segmentation scheme based on the improved deep learning U-Net model," *IEEE Access*, vol. 7, pp. 122634–122643, 2019, doi: 10.1109/ACCESS.2019.2935138.

[255] S. Yu, D. Xiao, S. Frost, and Y. Kanagasingam, "Robust optic disc and cup segmentation with deep learning for glaucoma detection," *Comput. Med. Imag. Graph.*, vol. 74, pp. 61–71, Jun. 2019, doi: 10.1016/j.compmedimag.2019.02.005.

[256] N. Liu, L. Liu, and J. Wang, "Local adaptive U-net for medical image segmentation," in *Proc. IEEE Int. Conf. Bioinf. Biomed. (BIBM)*, Dec. 2020, pp. 670–674, doi: 10.1109/BIBM49941.2020.9313515.

[257] W. Liu, H. Lei, H. Xie, B. Zhao, G. Yue, and B. Lei, "Multi-level light U-Net and atrous spatial pyramid pooling for optic disc segmentation on fundus image," in *Proc. Int. Workshop Ophthalmic Med. Image Anal.*, Jan. 2020, pp. 104–113.

[258] R. Kamble, P. Samanta, and N. Singhal, "Optic disc, cup and fovea detection from retinal images using U-Net++ with EfficientNet encoder," in *Proc. Int. Workshop Ophthalmic Med. Image Anal.*, Jan. 2020, pp. 93–103.

[259] G. A. Francia, C. Pedraza, M. Aceves, and S. Tovar-Arriaga, "Chaining a U-Net with a residual U-Net for retinal blood vessels segmentation," *IEEE Access*, vol. 8, pp. 38493–38500, 2020, doi: 10.1109/ACCESS.2020.2975745.

[260] R. Zhao, W. Chen, and G. Cao, "Edge-boosted U-Net for 2D medical image segmentation," *IEEE Access*, vol. 7, pp. 171214–171222, 2019.

[261] R. Adarsh, G. Amarnageswarao, R. Pandeeswari, and S. Deivalakshmi, "Dense residual convolutional auto encoder for retinal blood vessels segmentation," in *Proc. 6th Int. Conf. Adv. Comput. Commun. Syst. (ICACCS)*, Mar. 2020, pp. 280–284, doi: 10.1109/ICACCS48705.2020.9074172.

[262] Y. Wu, Y. Xia, Y. Song, D. Zhang, D. Liu, C. Zhang, and W. Cai, "Vessel-Net: Retinal vessel segmentation under multi-path supervision," in *Medical Image Computing and Computer Assisted Intervention*. Cham, Switzerland: Springer, 2019, pp. 264–272.

[263] H. H. Yu, X. Feng, Z. Wang, and H. Sun, "MixModule: Mixed CNN kernel module for medical image segmentation," in *Proc. IEEE 17th Int. Symp. Biomed. Imag. (ISBI)*, Apr. 2020, pp. 1508–1512, doi: 10.1109/ISBI45749.2020.9098498.

[264] K. Chen, G. Xu, J. Qian, and C.-X. Ren, "A bypass-based U-Net for medical image segmentation," in *Proc. Int. Conf. Intell. Sci. Big Data Eng.*, 2019, pp. 155–164.

[265] E. B. Kablan, H. Dogan, M. E. Ercin, S. Ersoz, and M. Ekinci, "An ensemble of fine-tuned fully convolutional neural networks for pleural effusion cell nuclei segmentation," *Comput. Electr. Eng.*, vol. 81, Jan. 2020, Art. no. 106533.

[266] T. Wan, L. Zhao, H. Feng, D. Li, C. Tong, and Z. Qin, "Robust nuclei segmentation in histopathology using ASPPU-net and boundary refinement," *Neurocomputing*, vol. 408, pp. 144–156, Sep. 2020, doi: 10.1016/j.neucom.2019.08.103.

[267] A. O. Vuola, S. U. Akram, and J. Kannala, "Mask-RCNN and U-Net ensembled for nuclei segmentation," in *Proc. IEEE 16th Int. Symp. Biomed. Imag. (ISBI)*, Apr. 2019, pp. 208–212.

[268] J. Zhao, L. Dai, M. Zhang, F. Yu, M. Li, H. Li, W. Wang, and L. Zhang, "PGU-Net+: Progressive growing of U-Net+ for automated cervical nuclei segmentation," in *Proc. Int. Workshop Multiscale Multimodal Med. Imag.*, 2019, pp. 51–58.

[269] B. Zhao, X. Chen, Z. Li, Z. Yu, S. Yao, L. Yan, Y. Wang, Z. Liu, C. Liang, and C. Han, "Triple U-Net: Hematoxylin-aware nuclei segmentation with progressive dense feature aggregation," *Med. Image Anal.*, vol. 65, Oct. 2020, Art. no. 101786, doi: 10.1016/j.media.2020.101786.

[270] Y. Huang, H. Zhu, P. Wang, and D. Dong, "Segmentation of overlapping cervical smear cells based on U-Net and improved level set," in *Proc. IEEE Int. Conf. Syst., Man Cybern. (SMC)*, Oct. 2019, pp. 3031–3035.

[271] M. Zhang, X. Li, M. Xu, and Q. Li, "RBC semantic segmentation for sickle cell disease based on deformable U-Net," in *Proc. Int. Conf. Med. Image Comput. Comput.-Assist. Intervent.*, 2018, pp. 695–702.

[272] C. E. Akbas and M. Kozubek, "Condensed U-Net (Cu-Net): An improved U-Net architecture for cell segmentation powered by 4×4 max-pooling layers," in *Proc. IEEE 17th Int. Symp. Biomed. Imag. (ISBI)*, Apr. 2020, pp. 446–450, doi: 10.1109/ISBI45749.2020.9098351.

[273] T. Overton and A. Tucker, "DO-U-Net for segmentation and counting," in *Proc. Int. Symp. Intell. Data Anal.*, 2020, pp. 391–403.

[274] D. Jha, M. A. Riegler, D. Johansen, P. Halvorsen, and H. D. Johansen, "DoubleU-Net: A deep convolutional neural network for medical image segmentation," in *Proc. IEEE 33rd Int. Symp. Comput.-Based Med. Syst. (CBMS)*, Jul. 2020, pp. 558–564, doi: 10.1109/CBMS49503.2020.00111.

[275] Y. Wang, Z. He, P. Xie, C. Yang, Y. Zhang, F. Li, X. Chen, K. Lu, T. Li, J. Zhou, and K. Zuo, "Segment medical image using U-Net combining recurrent residuals and attention," in *Medical Imaging and Computer-Aided Diagnosis*. Singapore: Springer, 2020, pp. 77–86.

[276] X. Li, Y. Huang, C. Yan, and L. Liu, "IT-block: Inverted triangle block embedded U-Net for medical image segmentation," in *Proc. Int. Joint Conf. Neural Netw. (IJCNN)*, Jul. 2020, pp. 1–8, doi: 10.1109/IJCNN48605.2020.9207047.

[277] R. M. Rad, P. Saeedi, J. Au, and J. Havelock, "Multi-resolutional ensemble of stacked dilated U-Net for inner cell mass segmentation in human embryonic images," in *Proc. 25th IEEE Int. Conf. Image Process. (ICIP)*, Oct. 2018, pp. 3518–3522.

[278] H. M. Saleh, N. H. Saad, and N. A. M. Isa, "Overlapping chromosome segmentation using U-Net: Convolutional networks with test time augmentation," *Procedia Comput. Sci.*, vol. 159, pp. 524–533, Jan. 2019.

[279] E. Altinsoy, C. Yilmaz, J. Wen, L. Wu, J. Yang, and Y. Zhu, "Raw G-band chromosome image segmentation using U-Net based neural network," in *Proc. Int. Conf. Artif. Intell. Soft Comput.*, 2019, pp. 117–126.

[280] H. Bai, T. Zhang, C. Lu, W. Chen, F. Xu, and Z.-B. Han, "Chromosome extraction based on U-Net and YOLOv3," *IEEE Access*, vol. 8, pp. 178563–178569, 2020, doi: 10.1109/ACCESS.2020.3026483.

[281] Y. M. Kassim, O. V. Glinskii, V. V. Glinsky, V. H. Huxley, G. Guidoboni, and K. Palaniappan, "Deep U-Net regression and hand-crafted feature fusion for accurate blood vessel segmentation," in *Proc. IEEE Int. Conf. Image Process. (ICIP)*, Sep. 2019, pp. 1445–1449.

[282] A. Ojeda-Pat, A. Martin-Gonzalez, and R. Soberanis-Mukul, "Convolutional neural network U-Net for trypanosoma Cruzi segmentation," in *Proc. Int. Symp. Intell. Comput. Syst.*, 2020, pp. 118–131.

[283] N. Ali, J. Kirchhoff, P. I. Onoja, A. Tannert, U. Neugebauer, J. Popp, and T. Bocklitz, "Predictive modeling of antibiotic susceptibility in E. Coli strains using the U-Net network and one-class classification," *IEEE Access*, vol. 8, pp. 167711–167720, 2020, doi: 10.1109/ACCESS.2020.3022829.

[284] G. Bueno, M. M. Fernandez-Carrobles, L. Gonzalez-Lopez, and O. Deniz, "Glomerulosclerosis identification in whole slide images using semantic segmentation," *Comput. Methods Programs Biomed.*, vol. 184, Feb. 2020, Art. no. 105273.

[285] X. Hu and H. Yang, "DRU-Net: A novel U-Net for biomedical image segmentation," *IET Image Process.*, vol. 14, no. 1, pp. 192–200, Jan. 2020.

[286] S. Li, J. Xu, and R. Chen, "U-Net neural network optimization method based on deconvolution algorithm," in *Proc. Int. Conf. Neural Inf. Process.*, Nov. 2020, pp. 592–602, doi: 10.1007/978-3-030-63830-6_50.

[287] M. E. Bagdigen and G. Bilgin, "Cell segmentation in triple-negative breast cancer histopathological images using U-Net architecture," in *Proc. 28th Signal Process. Commun. Appl. Conf. (SIU)*, Oct. 2020, pp. 1–4, doi: 10.1109/SIU49456.2020.9302367.

[288] J. Silva-Rodríguez, E. Payá-Bosch, G. García, A. Colomer, and V. Naranjo, "Prostate gland segmentation in histology images via residual and multi-resolution U-Net," in *Proc. Int. Conf. Intell. Data Eng. Automated Learn.*, Jan. 2020, pp. 1–8.

[289] M. Dash, N. D. Londhe, S. Ghosh, A. Semwal, and R. S. Sonawane, "PsLSNet: Automated psoriasis skin lesion segmentation using modified U-Net-based fully convolutional network," *Biomed. Signal Process. Control*, vol. 52, pp. 226–237, Jul. 2019.

[290] S. N. Hasan, M. Gezer, R. A. Azeez, and S. Gulsecen, "Skin lesion segmentation by using deep learning techniques," in *Proc. Med. Technol. Congr. (TIPTEKNO)*, Oct. 2019, pp. 1–4.

[291] Z. Al Nazi and T. A. Abir, "Automatic skin lesion segmentation and melanoma detection: Transfer learning approach with U-Net and DCNN-SVM," in *Proc. Int. Joint Conf. Comput. Intell.*, 2020, pp. 371–381.

[292] P. Tang, Q. Liang, X. Yan, S. Xiang, W. Sun, D. Zhang, and G. Coppola, "Efficient skin lesion segmentation using separable-unet with stochastic weight averaging," *Comput. Methods Programs Biomed.*, vol. 178, pp. 289–301, Sep. 2019.

[293] E. Z. Chen, X. Dong, X. Li, H. Jiang, R. Rong, and J. Wu, "Lesion attributes segmentation for melanoma detection with multi-task U-Net," in *Proc. IEEE 16th Int. Symp. Biomed. Imag. (ISBI)*, Apr. 2019, pp. 485–488.

[294] G. Asaeikheybari, J. Green, X. Qian, H. Jiang, and M.-C. Huang, "Medical image learning from a few/few training samples: Melanoma segmentation study," *Smart Health*, vol. 14, Dec. 2019, Art. no. 100088.

[295] L. Liu, L. Mou, X. X. Zhu, and M. Mandal, "Skin lesion segmentation based on improved U-Net," in *Proc. IEEE Can. Conf. Electr. Comput. Eng. (CCECE)*, May 2019, pp. 1–4.

[296] M. A. Al-masni, M. A. Al-antari, M.-T. Choi, S.-M. Han, and T.-S. Kim, "Skin lesion segmentation in dermoscopy images via deep full resolution convolutional networks," *Comput. Methods Programs Biomed.*, vol. 162, pp. 221–231, Aug. 2018.

[297] B. S. Lin, K. Michael, S. Kalra, and H. R. Tizhoosh, "Skin lesion segmentation: U-Nets versus clustering," in *Proc. IEEE Symp. Ser. Comput. Intell. (SSCI)*, Nov. 2017, pp. 1–7.

[298] D. R. Ramani and S. S. Ranjani, "U-Net based segmentation and multiple feature extraction of dermascopic images for efficient diagnosis of melanoma," in *Computer Aided Intervention and Diagnostics in Clinical and Medical Images*. Cham, Switzerland: Springer, 2019, pp. 81–101.

[299] B. Hafhouf, A. Zitouni, A. C. Megherbi, and S. Sbaa, "A modified U-Net for skin lesion segmentation," in *Proc. 1st Int. Conf. Commun., Control Syst. Signal Process. (CCSSP)*, May 2020, pp. 225–228, doi: 10.1109/CCSSP49278.2020.9151511.

[300] Y. Yang, C. Feng, and R. Wang, "Automatic segmentation model combining U-Net and level set method for medical images," *Expert Syst. Appl.*, vol. 153, Sep. 2020, Art. no. 113419, doi: 10.1016/j.eswa.2020.113419.

[301] D. Lin, Y. Li, T. L. Nwe, S. Dong, and Z. M. Oo, "RefineU-Net: Improved U-Net with progressive global feedbacks and residual attention guided local refinement for medical image segmentation," *Pattern Recognit. Lett.*, vol. 138, pp. 267–275, Oct. 2020, doi: 10.1016/j.patrec.2020.07.013.

[302] T. L. A. van den Heuvel, H. Petros, S. Santini, C. L. de Korte, and B. van Ginneken, "Automated fetal head detection and circumference estimation from free-hand ultrasound sweeps using deep learning in resource-limited countries," *Ultrasound Med. Biol.*, vol. 45, no. 3, pp. 773–785, Mar. 2019, doi: 10.1016/j.ultrasmedbio.2018.09.015.

[303] T. Włodarczyk, S. Plotka, T. Trzcinski, P. Rokita, N. Sochacki-Wójcicka, M. Lipa, and J. Wójcicki, "Estimation of preterm birth markers with U-Net segmentation network," in *Smart Ultrasound Imaging and Perinatal, Preterm and Paediatric Image Analysis*. Cham, Switzerland: Springer, 2019, pp. 95–103.

[304] B. Du, J. Wang, H. Zheng, C. Xiao, S. Fang, M. Lu, and R. Mao, "A novel transcranial ultrasound imaging method with diverging wave transmission and deep learning approach," *Comput. Methods Programs Biomed.*, vol. 186, Apr. 2020, Art. no. 105308, doi: 10.1016/j.cmpb.2019.105308.

[305] Y. Wang, C. Wei, Z.-J. Wang, Q.-G. Lu, and C.-G. Wang, "A more streamlined U-Net for nerve segmentation in ultrasound images," in *Proc. Chin. Automat. Congr. (CAC)*, Nov. 2018, pp. 101–104, doi: 10.1109/CAC.2018.8623052.

[306] Q. Zhang, Z. Cui, X. Niu, S. Geng, and Y. Qiao, "Image segmentation with pyramid dilated convolution based on ResNet and U-Net," in *Neural Information Processing*. Cham, Switzerland: Springer, 2017, pp. 364–372.

[307] N. Abraham, K. Illanko, N. Khan, and D. Androutsos, "Deep learning for semantic segmentation of brachial plexus nervesin ultrasound images using U-Net and M-Net," in *Proc. 3rd Int. Conf. Imag., Signal Process. Commun. (ICISPC)*, Jul. 2019, pp. 85–89, doi: 10.1109/ICISPC.2019.8935668.

[308] M. Amiri, R. Brooks, and H. Rivaz, "Fine tuning U-Net for ultrasound image segmentation: Which layers?" in *Domain Adaptation and Representation Transfer and Medical Image Learning with Less Labels and Imperfect Data*. Cham, Switzerland: Springer, 2019, pp. 235–242.

[309] M. Byra, P. Jarosik, A. Szubert, M. Galperin, H. Ojeda-Fournier, L. Olson, M. O'Boyle, C. Comstock, and M. Andre, "Breast mass segmentation in ultrasound with selective kernel U-Net convolutional neural network," *Biomed. Signal Process. Control*, vol. 61, Aug. 2020, Art. no. 102027, doi: 10.1016/j.bspc.2020.102027.

[310] M. Amiri, R. Brooks, B. Behboodi, and H. Rivaz, "Two-stage ultrasound image segmentation using U-Net and test time augmentation," *Int. J. Comput. Assist. Radiol. Surg.*, vol. 15, no. 6, pp. 981–988, Apr. 2020, doi: 10.1007/S11548-020-02158-3.

[311] J. Yang, M. Faraji, and A. Basu, "Robust segmentation of arterial walls in intravascular ultrasound images using dual path U-Net," *Ultrasonics*, vol. 96, pp. 24–33, Jul. 2019, doi: 10.1016/j.ultras.2019.03.014.

[312] M. Xie, Y. Li, Y. Xue, L. Huntress, W. Beckerman, S. Rahimi, J. Ady, and U. Roshan, "Vessel lumen segmentation in carotid artery ultrasounds with the U-Net convolutional neural network," in *Proc. IEEE Int. Conf. Bioinf. Biomed. (BIBM)*, Dec. 2020, pp. 2680–2684, doi: 10.1109/BIBM49941.2020.9313434.

[313] M. Xia, W. Yan, Y. Huang, Y. Guo, G. Zhou, and Y. Wang, "Extracting membrane borders in IVUS images using a multi-scale feature aggregated U-Net," in *Proc. 42nd Annu. Int. Conf. IEEE Eng. Med. Biol. Soc. (EMBC)*, Jul. 2020, pp. 1650–1653, doi: 10.1109/EMBC44109.2020.9175970.

[314] M. Xie, Y. Li, Y. Xue, L. Huntress, W. Beckerman, S. A. Rahimi, J. W. Ady, and U. W. Roshan, "Two-stage and dual-decoder convolutional U-Net ensembles for reliable vessel and plaque segmentation in carotid ultrasound images," in *Proc. 19th IEEE Int. Conf. Mach. Learn. Appl. (ICMLA)*, Dec. 2020, pp. 1376–1381, doi: 10.1109/ICMLA51294.2020.00214.

[315] S. Moradi, M. G. Oghli, A. Alizadehasl, I. Shiri, N. Oveisi, M. Oveisi, M. Maleki, and J. Dhooge, "MFP-UNet: A novel deep learning based approach for left ventricle segmentation in echocardiography," *Phys. Med.*, vol. 67, pp. 58–69, Nov. 2019.

[316] V. Zyuzin, A. Mukhtarov, D. Neustroev, and T. Chumarnaya, "Segmentation of 2D echocardiography images using residual blocks in U-Net architectures," in *Proc. Ural Symp. Biomed. Eng., Radioelectron. Inf. Technol. (USBEREIT)*, May 2020, pp. 499–502, doi: 10.1109/USBEREIT48449.2020.9117678.

[317] L. S. Hesse and A. I. L. Namburete, "Improving U-Net segmentation with active contour based label correction," in *Proc. Annu. Conf. Med. Image Understand. Anal.*, Jul. 2020, pp. 69–81, doi: 10.1007/978-3-030-52791-4_6.

[318] L. Xu, M. Liu, Z. Shen, H. Wang, X. Liu, X. Wang, S. Wang, T. Li, S. Yu, M. Hou, J. Guo, J. Zhang, and Y. He, "DW-Net: A cascaded convolutional neural network for apical four-chamber view segmentation in fetal echocardiography," *Comput. Med. Imag. Graph.*, vol. 80, Mar. 2020, Art. no. 101690, doi: 10.1016/j.compmedimag.2019.101690.

[319] X. Li, Y. Guo, F. Jiang, L. Xu, F. Shen, Z. Jin, and Y. Wang, "Multi-task refined boundary-supervision U-Net (MRBSU-Net) for gastrointestinal stromal tumor segmentation in endoscopic ultrasound (EUS) images," *IEEE Access*, vol. 8, pp. 5805–5816, 2020, doi: 10.1109/ACCESS.2019.2963472.

[320] J. Ding, Z. Huang, M. Shi, and C. Ning, "Automatic thyroid ultrasound image segmentation based on U-shaped network," in *Proc. 12th Int. Congr. Image Signal Process., Biomed. Eng. Informat. (CISP-BMEI)*, Oct. 2019, pp. 1–5, doi: 10.1109/CISP-BMEI48845.2019.8966062.

[321] S. Marques, C. Carvalho, C. Peixoto, D. Pignatelli, J. Beires, J. Silva, and A. Campilho, "Segmentation of gynaecological ultrasound images using different U-Net based approaches," in *Proc. IEEE Int. Ultrason. Symp. (IUS)*, Oct. 2019, pp. 1485–1488, doi: 10.1109/ULTSYM.2019.8925948.

[322] D. M. Alex and D. A. Chandy, "Investigations on performances of pre-trained U-Net models for 2D ultrasound kidney image segmentation," in *Proc. Int. Conf. Emerg. Technol. Comput.*, Aug. 2020, pp. 185–195, doi: 10.1007/978-3-030-60036-5_13.

[323] W. Zhang, H. Cheng, and J. Gan, "MUNet: A multi-scale U-Net framework for medical image segmentation," in *Proc. Int. Joint Conf. Neural Netw. (IJCNN)*, Jul. 2020, pp. 1–7, doi: 10.1109/IJCNN48605.2020.9206703.

[324] K. Hatano, S. Murakami, H. Lu, J. K. Tan, H. Kim, and T. Aoki, "Detection of phalange region based on U-Net," in *Proc. 18th Int. Conf. Control, Automat. Syst. (ICCAS)*, Oct. 2018, pp. 1338–1342.

[325] W. Wu, J. Zhang, H. Xie, Y. Zhao, S. Zhang, and L. Gu, "Automatic detection of coronary artery stenosis by convolutional neural network with temporal constraint," *Comput. Biol. Med.*, vol. 118, Mar. 2020, Art. no. 103657, doi: 10.1016/j.compbiomed.2020.103657.

[326] M. Gherardini, E. Mazomenos, A. Menciassi, and D. Stoyanov, "Catheter segmentation in X-ray fluoroscopy using synthetic data and transfer learning with light U-Nets," *Comput. Methods Programs Biomed.*, vol. 192, Aug. 2020, Art. no. 105420, doi: 10.1016/j.cmpb.2020.105420.

[327] L. Ding, K. Zhao, X. Zhang, X. Wang, and J. Zhang, "A lightweight U-Net architecture multi-scale convolutional network for pediatric hand bone segmentation in X-ray image," *IEEE Access*, vol. 7, pp. 68436–68445, 2019, doi: 10.1109/ACCESS.2019.2918205.

[328] M. Frid-Adar, A. Ben-Cohen, R. Amer, and H. Greenspan, "Improving the segmentation of anatomical structures in chest radiographs using U-Net with an ImageNet pre-trained encoder," in *Image Analysis for Moving Organ, Breast, and Thoracic Images*. Cham, Switzerland: Springer, 2018, pp. 159–168.

[329] S. Reza, O. B. Amin, and M. M. A. Hashem, "TransResUNet: Improving U-Net architecture for robust lungs segmentation in chest X-rays," in *Proc. IEEE Region Symp. (TENSYMP)*, Jun. 2020, pp. 1592–1595, doi: 10.1109/TENSYMP50017.2020.9230835.

[330] D. Waiker, P. D. Baghel, K. R. Varma, and S. P. Sahu, "Effective semantic segmentation of lung X-ray images using U-Net architecture," in *Proc. 4th Int. Conf. Comput. Methodol. Commun. (ICCMC)*, Mar. 2020, pp. 603–607, doi: 10.1109/ICCMC48092.2020.ICCMC-000112.

[331] Y. Shu, X. Wu, and W. Li, "LVC-Net: Medical image segmentation with noisy label based on local visual cues," in *Medical Image Computing and Computer Assisted Intervention*. Cham, Switzerland: Springer, 2019, pp. 558–566.

[332] Y. Mu, D. Xue, J. Guo, H. Xu, W. Wang, and H. Li, "Automatic calcaneus fracture identification and segmentation using a multi-task U-Net," in *Proc. 5th Int. Conf. Commun., Image Signal Process. (CCISP)*, Nov. 2020, pp. 140–144, doi: 10.1109/CCISP51026.2020.9273509.

[333] T. J. Jun, J. Kweon, Y.-H. Kim, and D. Kim, "T-Net: Nested encoder–decoder architecture for the main vessel segmentation in coronary angiography," *Neural Netw.*, vol. 128, pp. 216–233, Aug. 2020, doi: 10.1016/j.neunet.2020.05.002.

[334] H. Toda, Y. Iwahori, H. Usami, B. Kijsirikul, M. K. Bhuyan, N. Ogasawara, and K. Kasugai, "Shape recovery of polyp using blood vessel detection and matching estimation by U-Net," in *Proc. 8th Int. Congr. Adv. Appl. Informat. (IIAI-AAI)*, Jul. 2019, pp. 450–453.

[335] S. M. Kamrul Hasan and C. A. Linte, "U-NetPlus: A modified encoder-decoder U-Net architecture for semantic and instance segmentation of surgical instruments from laparoscopic images," in *Proc. 41st Annu. Int. Conf. IEEE Eng. Med. Biol. Soc. (EMBC)*, Jul. 2019, pp. 7205–7211.

[336] J. Leng, Y. Liu, T. Zhang, P. Quan, and Z. Cui, "Context-aware U-Net for biomedical image segmentation," in *Proc. IEEE Int. Conf. Bioinf. Biomed. (BIBM)*, Dec. 2018, pp. 2535–2538.

[337] D. J. Matuszewski and I.-M. Sintorn, "Reducing the U-Net size for practical scenarios: Virus recognition in electron microscopy images," *Comput. Methods Programs Biomed.*, vol. 178, pp. 31–39, Sep. 2019.

[338] J. I. Orlando, P. Seebock, H. Bogunovic, S. Klimscha, C. Grechenig, S. Waldstein, B. S. Gerendas, and U. Schmidt-Erfurth, "U2-Net: A Bayesian U-Net model with epistemic uncertainty feedback for photoreceptor layer segmentation in pathological OCT scans," in *Proc. IEEE 16th Int. Symp. Biomed. Imag. (ISBI)*, Apr. 2019, pp. 1441–1445, doi: 10.1109/ISBI.2019.8759581.

[339] Y. He, A. Carass, Y. Liu, B. M. Jedynak, S. D. Solomon, S. Saidha, P. A. Calabresi, and J. L. Prince, "Fully convolutional boundary regression for retina OCT segmentation," in *Proc. Int. Conf. Med. Image Comput. Comput.-Assist. Intervent.*, vol. 11764, Oct. 2019, pp. 120–128, doi: 10.1007/978-3-030-32239-7_14.

[340] J. Kugelman, D. Alonso-Caneiro, S. A. Read, S. J. Vincent, F. K. Chen, and M. J. Collins, "Effect of altered OCT image quality on deep learning boundary segmentation," *IEEE Access*, vol. 8, pp. 43537–43553, Jan. 2020, doi: 10.1109/ACCESS.2020.2977355.

[341] I. Z. Matovinovic, S. Loncaric, J. Lo, M. Heisler, and M. Sarunic, "Transfer learning with U-Net type model for automatic segmentation of three retinal layers in optical coherence tomography images," in *Proc. 11th Int. Symp. Image Signal Process. Anal. (ISPA)*, Sep. 2019, pp. 49–53, doi: 10.1109/ISPA.2019.8868639.

[342] S. Liu, D. P. Shamonin, G. Zahnd, A. F. W. van der Steen, T. van Walsum, and G. van Soest, "Healthy vessel wall detection using U-Net in optical coherence tomography," in *Machine Learning and Medical Engineering for Cardiovascular Health and Intravascular Imaging and Computer Assisted Stenting*. Cham, Switzerland: Springer, 2019, pp. 184–192.

[343] Z. Chen, D. Li, H. Shen, H. Mo, Z. Zeng, and H. Wei, "Automated segmentation of fluid regions in optical coherence tomography B-scan images of age-related macular degeneration," *Opt. Laser Technol.*, vol. 122, Feb. 2020, Art. no. 105830, doi: 10.1016/j.optlastec.2019.105830.

[344] R. Tennakoon, A. K. Gostar, R. Hoseinnezhad, and A. Bab-Hadiashar, "Retinal fluid segmentation in OCT images using adversarial loss based convolutional neural networks," in *Proc. IEEE 15th Int. Symp. Biomed. Imag.*, Apr. 2018, pp. 1436–1440, doi: 10.1109/ISBI.2018.8363842.

[345] R. Asgari, S. Waldstein, F. Schlanitz, M. Baratsits, U. Schmidt-Erfurth, and H. Bogunović, "U-Net with spatial pyramid pooling for drusen segmentation in optical coherence tomography," in *Ophthalmic Medical Image Analysis*. Cham, Switzerland: Springer, 2019, pp. 77–85.

[346] M. Zhang, C. Zhang, X. Wu, X. Cao, G. S. Young, H. Chen, and X. Xu, "A neural network approach to segment brain blood vessels in digital subtraction angiography," *Comput. Methods Programs Biomed.*, vol. 185, Mar. 2020, Art. no. 105159.

[347] R. Kimura, A. Teramoto, T. Ohno, K. Saito, and H. Fujita, "Virtual digital subtraction angiography using multizone patch-based U-Net," *Phys. Eng. Sci. Med.*, vol. 43, no. 4, pp. 1305–1315, Oct. 2020, doi: 10.1007/S13246-020-00933-9.

[348] S. Liu, Y. Li, J. Zhou, J. Hu, N. Chen, Y. Shang, Z. Chen, and T. Li, "Segmenting nailfold capillaries using an improved U-Net network," *Microvascular Res.*, vol. 130, Jul. 2020, Art. no. 104011, doi: 10.1016/j.mvr.2020.104011.

[349] Y. Han and J. C. Ye, "Framing U-Net via deep convolutional framelets: Application to sparse-view CT," *IEEE Trans. Med. Imag.*, vol. 37, no. 6, pp. 1418–1429, Jun. 2018.

[350] Y. Liu, B. Tracey, S. Aeron, E. Miller, T. Sun, N. McDannold, and J. Murphy, "Artifact suppression for passive cavitation imaging using U-Net CNNs with uncertainty quantification," in *Proc. IEEE 4th Int. Conf. Signal Image Process. (ICSIP)*, Jul. 2019, pp. 1037–1042, doi: 10.1109/SIPROCESS.2019.8868593.

[351] R. Souza, M. Bento, N. Nogovitsyn, K. J. Chung, W. Loos, R. M. Lebel, and R. Frayne, "Dual-domain cascade of U-Nets for multi-channel magnetic resonance image reconstruction," *Magn. Reson. Imag.*, vol. 71, pp. 140–153, Sep. 2020, doi: 10.1016/j.mri.2020.06.002.

[352] H. Lan, D. Jiang, C. Yang, F. Gao, and F. Gao, "Y-net: Hybrid deep learning image reconstruction for photoacoustic tomography *in vivo*," *Photoacoustics*, vol. 20, Dec. 2020, Art. no. 100197, doi: 10.1016/j.pacs.2020.100197.

[353] Z. Cheng, K. Guo, C. Wu, J. Shen, and L. Qu, "U-Net cascaded with dilated convolution for medical image registration," in *Proc. Chin. Automat. Congr. (CAC)*, Nov. 2019, pp. 3647–3651.

[354] M. Salem, S. Valverde, M. Cabezas, D. Pareto, A. Oliver, J. Salvi, À. Rovira, and X. Lladó, "A fully convolutional neural network for new T2-W lesion detection in multiple sclerosis," *NeuroImage, Clin.*, vol. 25, Jan. 2020, Art. no. 102149.

[355] D. Wei, L. Zhang, Z. Wu, X. Cao, G. Li, D. Shen, and Q. Wang, "Deep morphological simplification network (MS-Net) for guided registration of brain magnetic resonance images," *Pattern Recognit.*, vol. 100, Apr. 2020, Art. no. 107171, doi: 10.1016/j.patcog.2019.107171.

[356] B. R. Thomson, J. N. Smit, O. V. Ivashchenko, N. F. M. Kok, K. F. D. Kuhlmann, T. J. M. Ruers, and M. Fusaglia, "MR-to-US registration using multiclass segmentation of hepatic vasculature with a reduced 3D U-Net," in *Proc. Int. Conf. Med. Image Comput. Comput.-Assist. Intervent.*, Oct. 2020, pp. 275–284, doi: 10.1007/978-3-030-59716-0_27.

[357] L. Sun, D. Zhang, L. Wang, W. Shao, Z. Chen, W. Lin, D. Shen, and G. Li, "Topological correction of infant cortical surfaces using anatomically constrained U-Net," in *Proc. Int. Workshop Mach. Learn. Med. Imag.*, 2018, pp. 125–133.

[358] I. Olaciregui-Ruiz, I. Torres-Xirau, J. Teuwen, U. A. van der Heide, and A. Mans, "A deep learning-based correction to EPID dosimetry for attenuation and scatter in the unity MR-linac system," *Phys. Medica*, vol. 71, pp. 124–131, Mar. 2020.

[359] G. Li, L. Bai, C. Zhu, E. Wu, and R. Ma, "A novel method of synthetic CT generation from MR images based on convolutional neural networks," in *Proc. 11th Int. Congr. Image Signal Process., Biomed. Eng. Informat. (CISP-BMEI)*, Oct. 2018, pp. 1–5.

[360] O. Lucena, R. Souza, L. Rittner, R. Frayne, and R. Lotufo, "Convolutional neural networks for skull-stripping in brain MR imaging using silver standard masks," *Artif. Intell. Med.*, vol. 98, pp. 48–58, Jul. 2019.

[361] K. P. Murphy, *Machine Learning: A Probabilistic Perspective*. Cambridge, MA, USA: MIT Press, 2012.

[362] L. R. Dice, "Measures of the amount of ecologic association between species," *Ecology*, vol. 26, no. 3, pp. 297–302, Jul. 1945.

[363] P. Jaccard, "The distribution of the flora in the alpine zone.1," *New Phytologist*, vol. 11, no. 2, pp. 37–50, Feb. 1912.

[364] S. S. M. Salehi, D. Erdogmus, and A. Gholipour, "Tversky loss function for image segmentation using 3D fully convolutional deep networks," in *Proc. Int. Workshop Mach. Learn. Med. Imag.*, 2017, pp. 379–387.

[365] H. Kervadec, J. Bouchtiba, C. Desrosiers, E. Granger, J. Dolz, and I. B. Ayed, "Boundary loss for highly unbalanced segmentation," in *Proc. 2nd Int. Conf. Med. Imag. With Deep Learn.*, 2019, pp. 285–296.

[366] D. M. W. Powers, "Evaluation: From precision, recall and F-measure to ROC, informedness, markedness and correlation," 2020, *arXiv:2010.16061*. [Online]. Available: http://arxiv.org/abs/2010.16061

[367] T. Fawcett, "An introduction to ROC analysis," *Pattern Recognit. Lett.*, vol. 27, no. 8, pp. 861–874, Jun. 2006.

[368] G. Litjens, T. Kooi, B. E. Bejnordi, A. A. A. Setio, F. Ciompi, M. Ghafoorian, J. A. Van Der Laak, B. Van Ginneken, and C. I. Sánchez, "A survey on deep learning in medical image analysis," *Med. Image Anal.*, vol. 42, pp. 60–88, Dec. 2017.

[369] M. Bakator and D. Radosav, "Deep learning and medical diagnosis: A review of literature," *Multimodal Technol. Interact.*, vol. 2, no. 3, p. 47, 2018.

[370] T. Nair, D. Precup, D. L. Arnold, and T. Arbel, "Exploring uncertainty measures in deep networks for multiple sclerosis lesion detection and segmentation," *Med. Image Anal.*, vol. 59, p. 101557, 2020.

[371] X. Xia and B. Kulis, "W-Net: A deep model for fully unsupervised image segmentation," 2017, *arXiv:1711.08506*. [Online]. Available: http://arxiv.org/abs/1711.08506

[372] Z. Khan and J. Yang, "Bottom-up unsupervised image segmentation using FC-dense U-Net based deep representation clustering and multi-dimensional feature fusion based region merging," *Image Vis. Comput.*, vol. 94, Feb. 2020, Art. no. 103871.

[373] F. Chen, Y. Jiang, X. Zeng, J. Zhang, X. Gao, and M. Xu, "PUB-SalNet: A pre-trained unsupervised self-aware backpropagation network for biomedical salient segmentation," *Algorithms*, vol. 13, no. 5, p. 126, 2020.

[374] M. Tan and Q. V. Le, "EfficientNet: Rethinking model scaling for convolutional neural networks," 2019, *arXiv:1905.11946*. [Online]. Available: http://arxiv.org/abs/1905.11946
[375] X. Yi, E. Walia, and P. Babyn, "Generative adversarial network in medical imaging: A review," *Med. Image Anal.*, vol. 58, Dec. 2019, Art. no. 101552.
[376] N. Papernot, P. McDaniel, I. Goodfellow, S. Jha, Z. B. Celik, and A. Swami, "Practical black-box attacks against machine learning," in *Proc. ACM Asia Conf. Comput. Commun. Secur.*, 2017, pp. 506–519.
[377] M. I. Razzak, S. Naz, and A. Zaib, "Deep learning for medical image processing: Overview, challenges and the future," in *Classification BioApps*. Cham, Switzerland: Springer, 2018, pp. 323–350.
[378] World Health Organization. *Weekly Operational Update on COVID-19 2 October 2020*. Accessed: Oct. 7, 2020. [Online]. Available: https://www.who.int/publications/m/item/weekly-update-on-covid-19—2-october-2020
[379] B. Wang *et al.*, "AI-assisted CT imaging analysis for COVID-19 screening: Building and deploying a medical AI system," *Appl. Soft Comput.*, vol. 98, Jan. 2021, Art. no. 106897, doi: 10.1016/j.asoc.2020.106897.
[380] X. Chen, L. Yao, and Y. Zhang, "Residual attention U-Net for automated multi-class segmentation of COVID-19 chest CT images," 2020, *arXiv:2004.05645*. [Online]. Available: http://arxiv.org/abs/2004.05645
[381] T. Zhou, S. Canu, and S. Ruan, "An automatic COVID-19 CT segmentation based on U-Net with attention mechanism," 2020, *arXiv:2004.06673*. [Online]. Available: https://arxiv.org/abs/2004.06673
[382] Y.-H. Wu, S.-H. Gao, J. Mei, J. Xu, D.-P. Fan, R.-G. Zhang, and M.-M. Cheng, "JCS: An explainable COVID-19 diagnosis system by joint classification and segmentation," 2020, *arXiv:2004.07054*. [Online]. Available: http://arxiv.org/abs/2004.07054
[383] Q. Yan, B. Wang, D. Gong, C. Luo, W. Zhao, J. Shen, Q. Shi, S. Jin, L. Zhang, and Z. You, "COVID-19 chest CT image segmentation—A deep convolutional neural network solution," 2020, *arXiv:2004.10987*. [Online]. Available: https://arxiv.org/abs/2004.10987
[384] G. Gaál, B. Maga, and A. Lukács, "Attention U-Net based adversarial architectures for chest X-ray lung segmentation," 2020, *arXiv:2003.10304*. [Online]. Available: http://arxiv.org/abs/2003.10304
[385] T. Ozturk, M. Talo, E. A. Yildirim, U. B. Baloglu, O. Yildirim, and 'U. R. Acharya, "Automated detection of COVID-19 cases using deep neural networks with X-ray images," *Comput. Biol. Med.*, vol. 121, Jun. 2020, Art. no. 103792.
[386] M. Z. Alom, M. M. S. Rahman, M. S. Nasrin, T. M. Taha, and V. K. Asari, "COVID_MTNet: COVID-19 detection with multi-task deep learning approaches," 2020, *arXiv:2004.03747*. [Online]. Available: http://arxiv.org/abs/2004.03747
[387] F. Shi, J. Wang, J. Shi, Z. Wu, Q. Wang, Z. Tang, K. He, Y. Shi, and D. Shen, "Review of artificial intelligence techniques in imaging data acquisition, segmentation, and diagnosis for COVID-19," *IEEE Rev. Biomed. Eng.*, vol. 14, pp. 4–15, 2021.

NAHIAN SIDDIQUE (Graduate Student Member, IEEE) received the B.S. degree in electrical and electronic engineering from the Islamic University of Technology, Bangladesh, in 2017. He is currently pursuing the M.S. degree in electrical and computer engineering with Purdue University Northwest. His current research interests include deep learning, computer vision, biomedical image processing, and remote sensing.

SIDIKE PAHEDING received the Ph.D. degree in electrical engineering from the University of Dayton. He is currently an Assistant Professor with the Department of Applied Computing, Michigan Technological University. Prior to joining Michigan Tech, in 2020, he was a Visiting Assistant Professor with Purdue University Northwest. His research interests include image/video processing, machine learning, deep learning, computer vision, and remote sensing. He is an Associate Editor of the *Signal, Image and Video Processing* (Springer), and *Photogrammetric Engineering & Remote Sensing* (ASPRS), and serves as a guest editor/a reviewer for several reputed journals.

COLIN P. ELKIN (Member, IEEE) received the B.S. degree in electrical engineering from The University of Tulsa, in 2013, and the M.S. and Ph.D. degrees in computer science and engineering from The University of Toledo, in 2015 and 2018, respectively. His Ph.D. dissertation was supported by the Air Force Research Laboratory (AFRL) through two research awards, a Dayton Area Graduate Studies Institute (DAGSI) Fellowship and an AFRL subcontract through Soar Technology, Inc. In 2018, he joined the Department of Electrical and Computer Engineering, Purdue University Northwest, as a Visiting Instructor and a Visiting Assistant Professor. He has been an Assistant Professor, since 2019. He has published more than ten peer-reviewed conferences, journals, and poster papers. His past and present research has been funded by the Department of Defense (DoD), NSF, the Ohio Federal Research Network (OFRN), and industry. His research interests include artificial intelligence, data science, machine learning, optimization techniques, human factors, modeling and simulation, engineering education, and software engineering.

VIJAY DEVABHAKTUNI (Senior Member, IEEE) received the B.Eng. degree in electronics and electrical engineering and the M.Sc. degree in physics from the Birla Institute of Technology and Science, Pilani, India, in 1996, and the Ph.D. degree in electronics from Carleton University, Ottawa, ON, Canada, in 2003. He held the Natural Sciences and Engineering Research Council of Canada (NSERC) Postdoctoral Fellowship and spent the tenure researching with Dr. J. W. Haslett with the University of Calgary, Calgary, AB, Canada, from 2003 to 2004. In 2005, he taught at Penn State Behrend, Erie, PA, USA. From 2005 to 2008, he held the prestigious Canada Research Chair in computer-aided high-frequency modeling and design with Concordia University, Montréal, QC, Canada. In Summer of 2008, he joined the Department of Electrical Engineering and Computer Science, The University of Toledo, Toledo, OH, USA, as an Associate Professor, where he was promoted to a Professor, in 2013. In 2018, he joined as the Chair of the Department of Electrical and Computer Engineering, Purdue University Northwest, Hammond, IN, USA. He has coauthored 250 peer reviewed articles. He secured external funding close to U.S. five million in his research areas (sponsoring agencies include AFOSR, AFRL, CFI, NASA, NIST, NSERC, NSF, ONR, and industry). His research interests include applied electromagnetics, biomedical applications of wireless sensor networks, computer aided design, device modeling, image processing, infrastructure monitoring, neural networks, RF/microwave optimization, unmanned aerial vehicles (UAVs), and virtual reality. In Canada and USA, he graduated 75 thesis students at both M.S. and Ph.D. levels.